

# Fracture indentation beneath flat and spherical punches

R. MOUGINOT

*Etablissement Technique Central de l'Armement, 16 bis Av. Prieur de la Côte d'Or, 94114 Arcueil Cedex, France*

D. MAUGIS

*Equipe de recherche CNRS ER259, Mécanique des Surfaces, LCPC, 58 Bd Lefebvre, 75015 Paris, France*

The mechanics of crack initiation and propagation beneath an axisymmetric flat punch are investigated. The stress tensor given by Sneddon in 1946 is described. Numerical integration along stress trajectories gives the strain energy release rate as a function of both the crack length and its position relative to the indenter. Comparison with Hertzian fracture is made. The initiation of crack outside the circle of contact is shown to be due to the steepest gradient of stresses along the flaws near the circle of contact. The meaning of Auerbach's law is discussed. The Auerbach range is shown to correspond to the relatively flat maximum of the envelope of the  $G$  against  $c/a$  curves for various starting radii. The influence of subcritical crack growth is also discussed. The model proposed in 1978 by Maugis and Barquins for kinetics of crack propagation between punches and viscoelastic solids is used. It is assumed that the static fatigue limit corresponds to the true Griffith criterion with intrinsic surface energy  $\gamma$ , and that the critical strain energy release rate  $G_c$  corresponds to a criterion for crack speed instability and velocity jump, so that no stress corrosion is needed to explain subcritical crack growth for  $2\gamma < G < G_c$ . The 1971 experimental results of Mikoszà and Lawn are easily interpreted by this model. Finally, experiments performed on a borosilicate glass give results that agree satisfactorily with the theory. Due to kinetic effects, an apparent surface energy of about  $4.5 \text{ J m}^{-2}$  is obtained, larger than the intrinsic surface energy and slightly lower than the fracture energy derived from high-speed experiments.

## 1. Introduction

Since the early work of Auerbach [1], fracture of brittle solids by spherical indenters has been extensively studied. The mechanism of cone crack initiation and propagation is relatively well understood by using the Hertz-Huber stress tensor [2, 3] and fracture mechanics [4-6]. However the Hertzian fracture test, despite its simplicity, presents some drawbacks: the area of contact increases with load, and the surface trace of the crack cone can be enveloped by the expanding contact circle, causing secondary

fractures and application of the load both on the cone and the half-space. Furthermore, stress trajectories move as the radius of contact increases, rendering the analysis more delicate. As recognized by Roesler [7], cylindrical, flat-ended punches are better, and this geometry was used to give a constant radius of contact and to study the well-formed cone crack [7-12]. However, the theoretical analysis of fracture indentation by flat punches has never been done, most probably because the authors were unaware of the stress tensor computed by Sneddon [13]. This

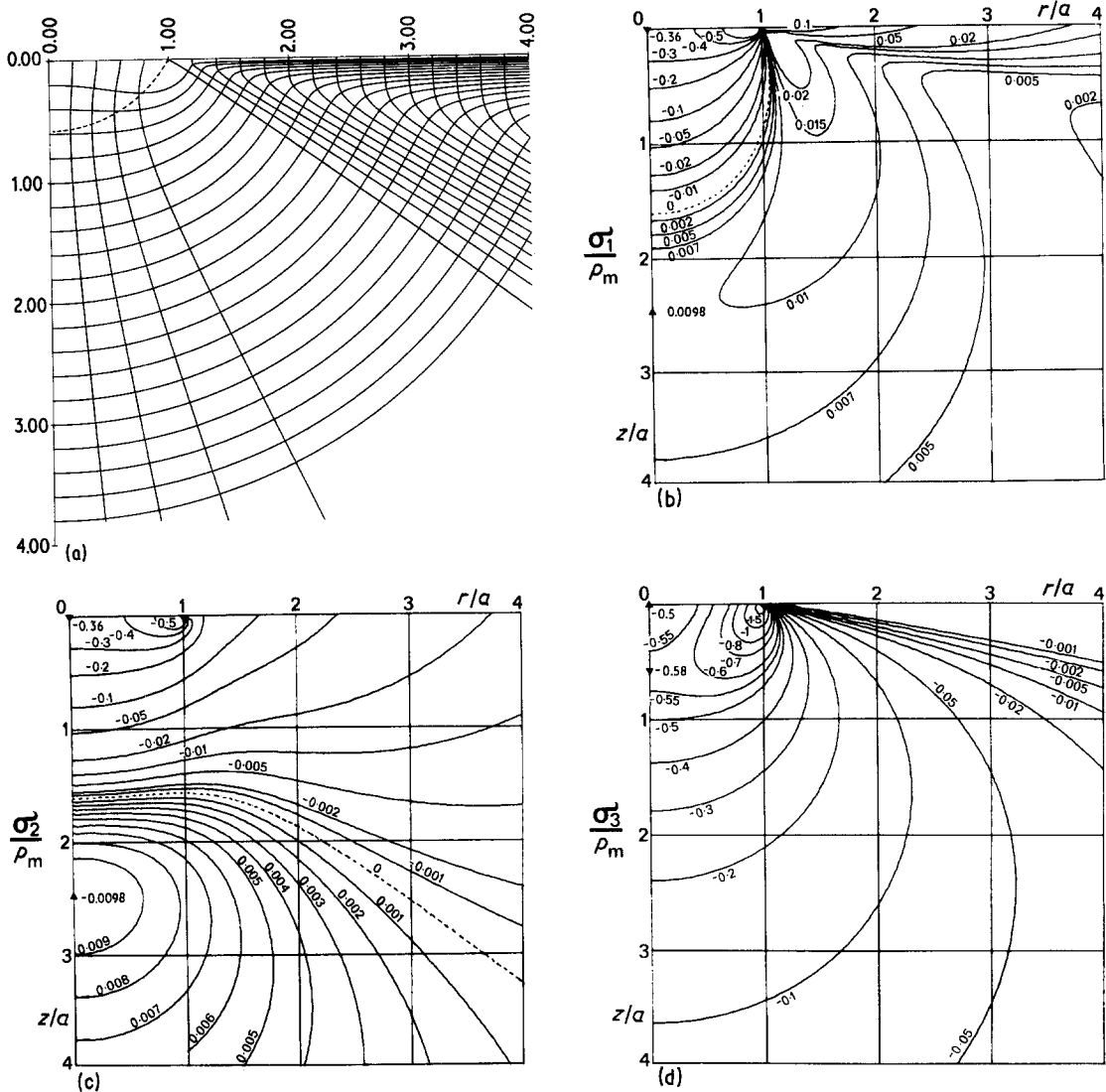


Figure 1 Stress trajectories (a) and contours of the reduced principal stresses (b, c, d) for a flat punch ( $\nu = 0.22$ ).

work is done here, and the fracture indentation by a flat punch is compared with the Hertzian fracture for a material with  $\nu = 0.22$ , the Poisson ratio of the optical glass used for experimental verifications.

### 2. The flat punch stress field

This stress field has been given by Sneddon [13] (with misprints later corrected by Barquins and Maugis [14]). Figs. 1 and 2 compare stress trajectories and contours of the reduced principal stress  $\sigma/p_m$  (where  $p_m = P/\pi a^2$  is the mean pressure) for the flat punch and the sphere. Stress trajectories exhibit vertical and horizontal tangents beneath the punch (isocline  $0^\circ$  in dashed

lines). Following Lawn [15] the principal stresses  $\sigma_1, \sigma_2, \sigma_3$  are so labelled that  $\sigma_1 > \sigma_2 > \sigma_3$  nearly everywhere and  $\sigma_2$  is the hoop stress. At the edge of the flat punch stresses are infinite, but outside the circle of contact the surface stresses and the surface displacements are the same as for the sphere. According to a proof by Way [16] they are independent of the stress distribution inside the circle of contact and are those of a concentrated force:

$$\sigma_1 = \frac{1 - 2\nu P}{2\pi r^2} \quad (1a)$$

$$\sigma_2 = -\frac{1 - 2\nu P}{2\pi r^2} \quad (1b)$$

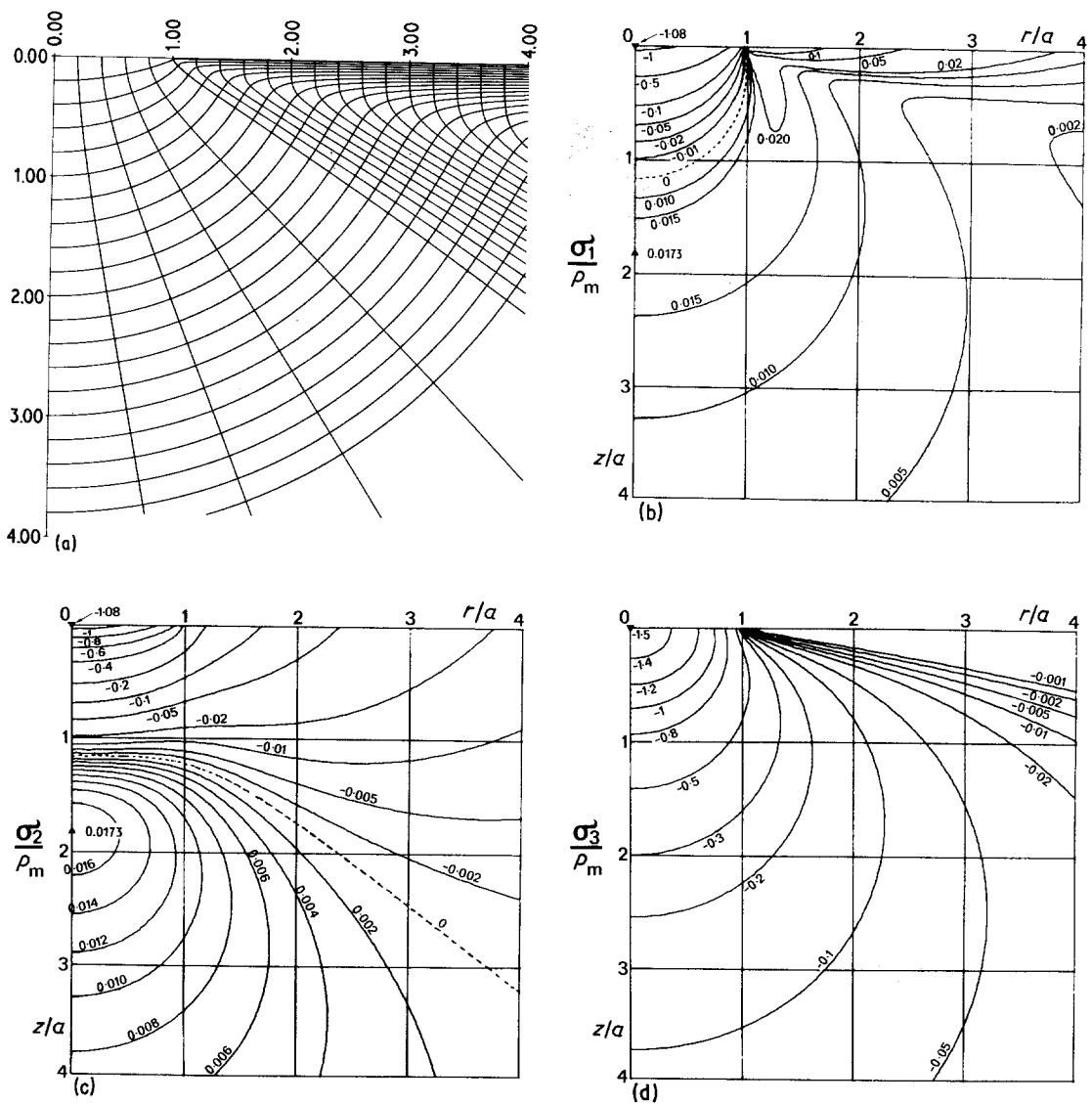


Figure 2 Stress trajectories (a) and contours of the reduced principal stresses (b, c, d) for a spherical punch ( $\nu = 0.22$ ).

At large distance from the origin the stress field is that of the Boussinesq concentrated force (depicted by Lawn and Swain [17]) according to the St Venant principle.

Figs. 3 and 4 compare the distribution of stress  $\sigma_1$  as a function of relative distance  $c/a$  along the stress trajectories starting at various values of  $r_0/a$ , for the flat punch and the sphere: the stress falls more rapidly with the flat punch, especially near the edge of the contact. It can thus be anticipated that a surface flaw just near the edge of the contact can hardly be activated by the tensile stress acting along it in comparison with outer surface flaws.

### 3. Fracture analysis

Let us assume, as usually, that the crack follows the  $\sigma_3$  trajectory starting at radius  $r_0 > a$  (Fig. 5). The initial growth is thus close to vertically downward, with a constant crack front  $2\pi r_0$ ; then the crack path widens following a cone with a crack front  $2\pi r_c$  constantly lengthening. The analysis generally done for Hertzian crack initiation [4-6] uses for the stress intensity factor the equation

$$K_I = 2 \left( \frac{c}{\pi} \right)^{1/2} \int_0^c \frac{\sigma(b)db}{(c^2 - b^2)^{1/2}} \quad (2a)$$

derived for an internal crack of length  $2c$  in an

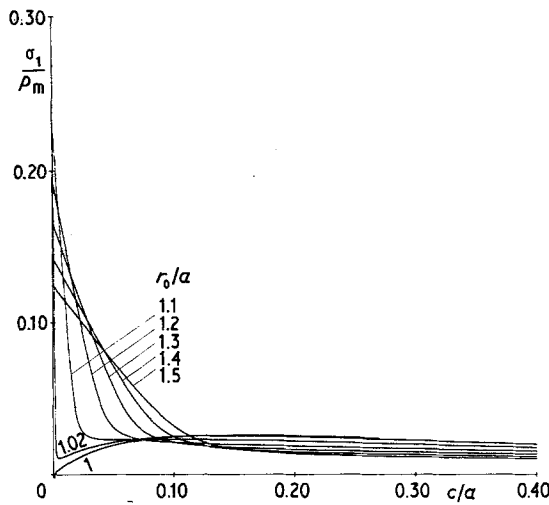


Figure 3 Flat punch ( $\nu = 0.22$ ). Distribution of stress  $\sigma_1$  as a function of relative distance  $c/a$  along the  $\sigma_3$  trajectories starting at various  $r_0/a$ .

infinite plate, the crack being subject to a normal stress  $\sigma(b)$  that varies along its length. This formula is also correct for a ring-shaped crack, but for a cone  $\sigma(b)$  acts on a ring of length  $2\pi r_b$ , while  $K_I$  refers to points on the crack front of length  $2\pi r_c$  that suffer less intensification of stress than a crack front of constant length. In this case, as suggested by our referee, it is better to write

$$K_I = 2 \left( \frac{c}{\pi} \right)^{1/2} \int_0^c \frac{r_b}{r_c} \frac{\sigma(b) db}{(c^2 - b^2)^{1/2}} \quad (2b)$$

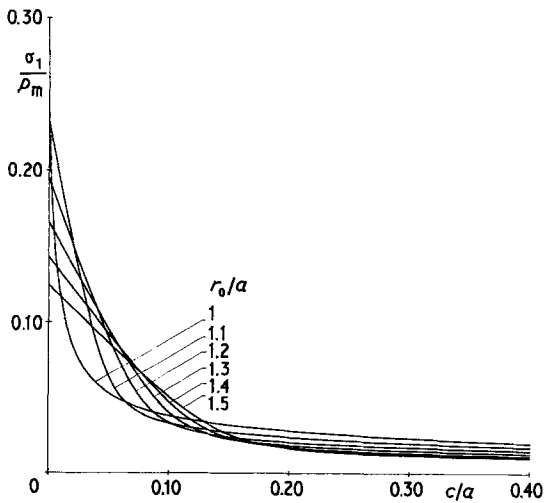


Figure 4 Spherical punch ( $\nu = 0.22$ ). Distribution of stress  $\sigma_1$  as a function of relative distance  $c/a$  along the  $\sigma_3$  trajectories for various  $r_0/a$ .

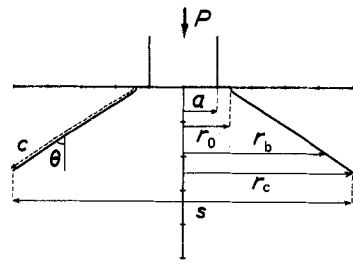


Figure 5 The well-formed cone ( $\nu = 0.22$ ,  $r_0/a = 1.4$ ,  $c/a = 4.5$ ).

Equation 2b has the advantage to reduce to Equation 2a for crack initiation, and to be consistent for a complete cone ( $r_b/r_c = b/c$ ) with the well-known formula for a penny-shaped crack (see Barenblatt [18] p. 96 and Rice [19]); i.e. for cone of semi-angle  $\pi/2$

$$K_I = \frac{2}{(\pi c)^{1/2}} \int_0^c \frac{b \sigma(b) db}{(c^2 - b^2)^{1/2}} \quad (2c)$$

Another difficulty arises from the fact that in many cases, especially in the Auerbach range (see Section 10.1), the crack does not develop symmetrically down from the surface, but rather gently runs round the contact area from a flow, to form a complete circle. This is difficult to analyse by fracture mechanics, and in the following we will always assume that axial symmetry holds.

As for any tridimensional crack, the plane strain formula applies [20] and the strain energy release rate is

$$G = \frac{1 - \nu^2}{E} K_I^2 \quad (3)$$

For a flat punch, as well as for a sphere, the stresses can be normalized by the mean pressure, and have the general form

$$\sigma \left( \frac{r}{a}, \frac{z}{a} \right) = \frac{P}{\pi a^3} f \left( \frac{r}{a}, \frac{z}{a} \right) \quad (4)$$

so that  $G$  has the general form

$$G = \frac{4}{\pi^3} \frac{1 - \nu^2}{E} \frac{P^2}{a^3} \left[ \Phi \left( \frac{c}{a} \right) \right]_{r_0/a, \nu} \quad (5)$$

with

$$\left[ \Phi \left( \frac{c}{a} \right) \right]_{r_0/a, \nu} = \frac{c}{a} \left[ \int_0^{c/a} \frac{r_b}{r_c} \frac{f \left( \frac{b}{a} \right) d \left( \frac{b}{a} \right)}{\left( \frac{c^2}{a^2} - \frac{b^2}{a^2} \right)^{1/2}} \right]^2 \quad (6)$$

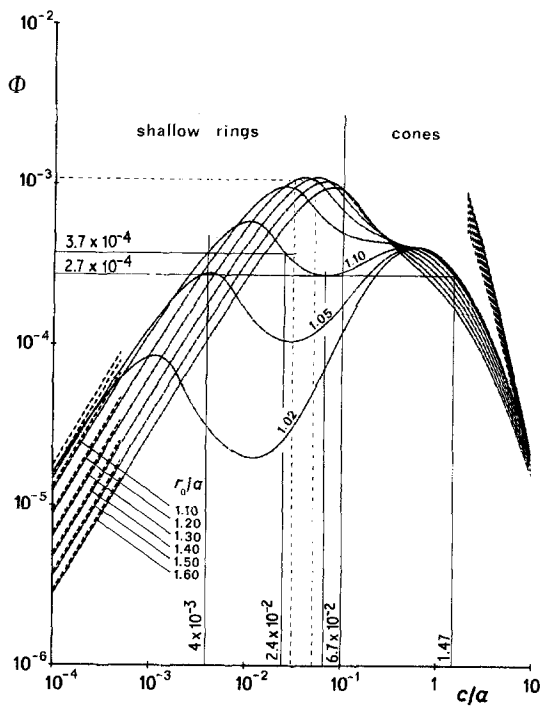


Figure 6 Flat punch ( $\nu = 0.22$ ). Strain energy release rate function  $\Phi(c/a)$  for various starting locations at the surface. Dashed lines: undiminishing stress field approximation for small  $c/a$ ; Roesler approximation for large  $c/a$ .

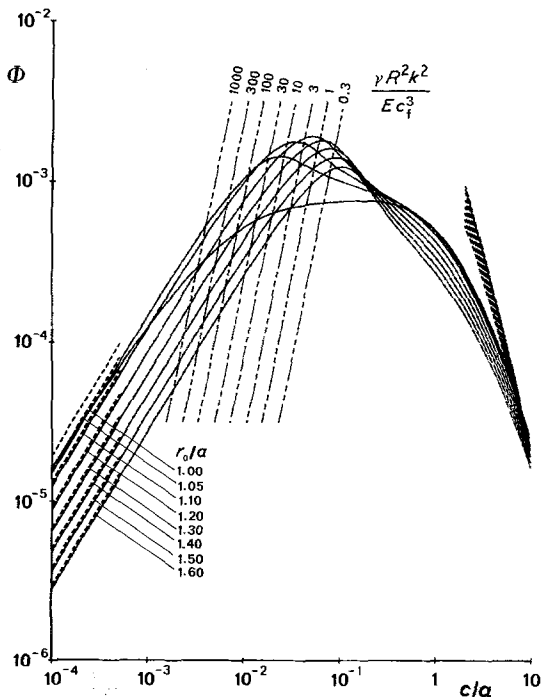


Figure 7 Spherical punch ( $\nu = 0.22$ ). Strain energy release rate function  $\Phi(c/a)$  for various starting locations at the surface. Dashed lines: undiminishing stress field approximation for small  $c/a$ ; Roesler approximation for large  $c/a$ .

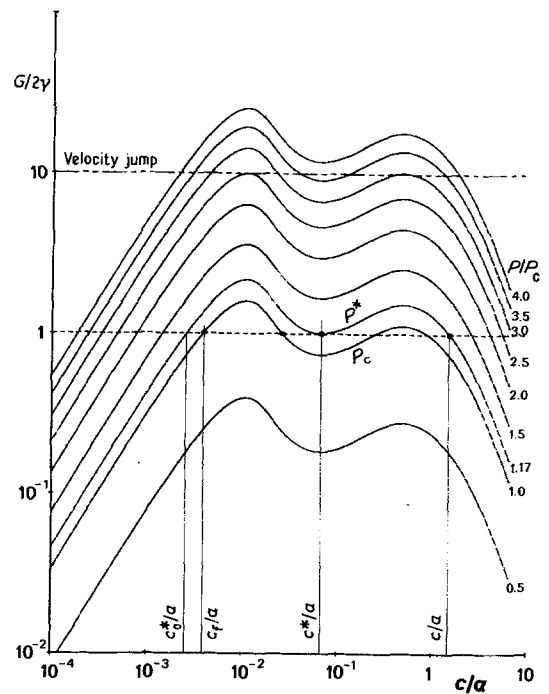


Figure 8 Flat punch ( $\nu = 0.22$ ). Reduced strain energy release rate against  $c/a$  for various loads. Starting radius of crack:  $r_0/a = 1.10$ .

For very small  $c/a$ ,  $\sigma(b)$  can be considered as a constant along the crack, with  $f(b/a) = (1 - 2\nu)a^2/2r_0^2$  given by Equation 1, and integration of Equation 6 with  $r_b = r_c$  gives

$$G = \frac{1 - \nu^2}{\pi} \left( \frac{1 - 2\nu}{2} \right)^2 \frac{P^2}{Ea^3} \left( \frac{a}{r_0} \right)^4 \frac{c}{a} \quad (7)$$

independent of the punch geometry. Otherwise the function  $\Phi(c/a)$  is obtained by numerical integration of Equation 6. The results are compared in Figs. 6 and 7 for the flat punch and the sphere, for  $\nu = 0.22$  and various starting values  $r_0/a$ . For the sphere the curves display a single maximum, whereas for the flat punch two maxima appear for  $r_0/a < 1.2$ .

## 4. Initiation of fracture

### 4.1. Curves with two maxima

In this case the analysis is similar to that given by Frank and Lawn [4] and Langitan and Lawn [21] for the sphere. Consider (Fig. 8) the curve  $G/2\gamma$  against  $c/a$  for a given initial value  $r_0/a$ . The equilibrium corresponds to  $G/2\gamma = 1$ , and this equilibrium is unstable on a branch with positive slope, and stable on a branch with negative one. Let  $P^*$  be the load whose hump reaches the line

$G/2\gamma = 1$ , and  $c_0^*/a$  and  $c^*/a$  the abscissae of the two left-hand intersections.

Let us consider a surface flaw of length  $c_f$  situated at  $r/a$  and such that  $c_0^* < c_f < c^*$ . By increasing the load,  $G$  at the crack tip increases until  $G = 2\gamma$ . At this point the load is given by

$$P_c = \left( \frac{\pi^3 E \gamma}{2(1 - \nu^2)} \right)^{1/2} \left( \frac{a^3}{[\Phi(c_f/a)]_{r_0/a}} \right)^{1/2} \quad (8)$$

If at this point the slope is negative, the flaw is in stable equilibrium; if it is positive,  $G$  increases at constant load  $P_c$  and the crack spontaneously extends, taking the energy from the elastic field. When the first maximum is reached,  $G$  then decreases and the crack slows down (see Section 11) on the stable branch until  $G/2\gamma = 1$  again and then stops, forming a shallow ring around the punch. On increasing the load further, the crack extends in a stable manner with the load, until  $c = c^*$  and  $P = P^*$ . At this stage the shallow ring becomes unstable, and as above the crack accelerates and then decelerates at constant load  $P^*$  forming a well-developed stable cone when it stops at  $G = 2\gamma$ . The critical load for initiation of the cone is thus  $P^*$ , given by

$$P^* = \left( \frac{\pi^3 E \gamma}{2(1 - \nu^2)} \right)^{1/2} \left( \frac{a^3}{[\Phi(c^*/a)]_{r_0/a}} \right)^{1/2} \quad (9)$$

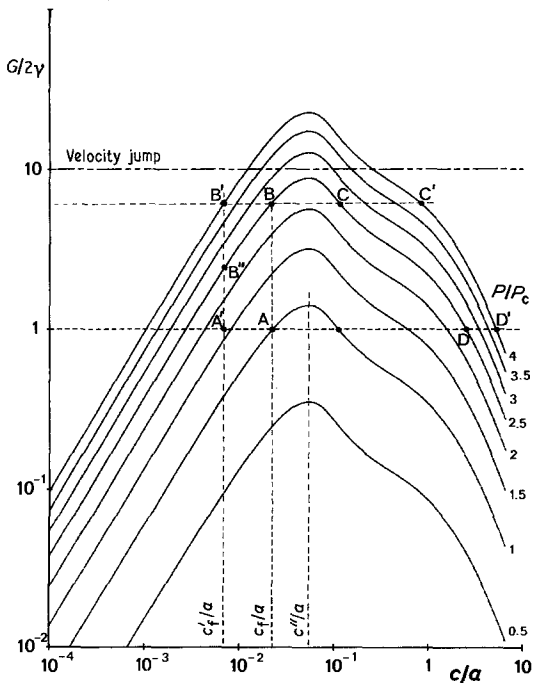


Figure 9 Flat punch ( $\zeta = 0.22$ ). Reduces strain energy release rate against  $c/a$  for various loads. Starting radius of the crack:  $r_0/a = 1.40$ .

This load can be independent of the initial flaw size, with the sole condition that the starting radius  $r_0/a$  be independent of the flaw size.

If the surface flaw at  $r_0/a$  is such that  $c_f < c_0^*$ , the equilibrium load given by Equation 8 is larger than  $P^*$ , and as this equilibrium is unstable  $G$  increases and then decreases, increases anew and decreases, passing through two maxima and giving directly the well-formed cone. The critical load is still given by Equation 8. For such a small flaw, the undiminishing stress field approximation of Equation 7 can be used, giving

$$P_c = \left( \frac{8\pi E \gamma}{(1 - \nu^2)(1 - 2\nu)^2} \right)^{1/2} \left( \frac{a}{c_f} \right)^{1/2} \left( \frac{r_0}{a} \right)^2 a^{3/2} \quad (10)$$

independent of the punch geometry. For a sphere, this reduces to Equation 17 of Wilshaw [22] (except for the factor 1.12), i.e.  $P_c$  varying as  $R^2(r_0/a)^6$ .

#### 4.2. Curves with a single maximum

Let  $c''/a$  be the abscissa of the maximum for a given value of  $r_0/a$  (Fig. 9). If  $c_f/a < c''/a$  (small flaws or punch of large radius),  $G$  increases at the crack tip as the load increases until  $G = 2\gamma$  at the load  $P_c$  given by Equation 8. The equilibrium is thus unstable and at the constant load  $P_c$ ,  $G$  increases and then decreases, with the crack accelerating and then slowing down until  $G = 2\gamma$  is reached anew. A shallow ring or a cone thus appears at this critical load  $P_c$ . The smaller the initial flaws, or the larger the punch, the greater the cone formed.

If  $c_f/a > c''/a$  (large flaws or small punch), the flaw at  $r_0/a$  is in stable equilibrium as soon as  $G = 2\gamma$ , and the crack extends in stable manner when the load increases further. In this case the critical load is difficult to detect.

#### 5. The starting radius of the crack

The critical load for crack initiation depends strongly on the starting radius  $r_0/a$  of the crack. This is clearly visible in Equation 10 for the undiminishing stress field. At this stage it is not possible to say that the critical load  $P^*$  corresponding to the hump is independent of the flaw size, as often quoted, since  $\Phi(c^*/a)$  depends on  $r_0/a$ .

In Hertzian fracture it has been long recognized [22–28] that the cone does not initiate at

the edge of the contact, but at larger  $r_0/a$ , say 1.1 to 1.4, the value increasing as the ball radius  $R$  decreases [26, 27], or the abrasion increases [28]. The same behaviour is observed for the flat punch, but with  $r_0/a$  still higher (see below). Two kinds of explanation have been proposed. The first, by Johnson *et al.* [27], is that an interfacial shear stress appears due to elastic mismatch, causing the maximum surface tensile stress to diminish and to move outwards from the contact circle. However experiments with lubricated contacts [24] do not give a significantly different result, and experiments without elastic mismatch [27] still give  $r_0/a > 1$ . The other explanation is based on a Weibull distribution of flaws in the undiminishing stress field approximation [26, 29] but three parameters must be adjusted by best fit with experimental results.

A more simple explanation is proposed here, based on remarks by Nadeau [30] and Lawn *et al.* [31]. They noted that, as the stress gradient is steepest close the contact circle, the flaws were more likely to grow at a larger  $r_0/a$  where the tension remains reasonably high along its entire length; for small  $c_f$  the starting point of the cone crack is very close to the contact circle, while for large  $c_f$  it lies well outside [31]. Similar remarks were made later by Warren [6].

Figs. 10 and 11 display, for various given values of  $c_f/a$ , the variation of the function  $\Phi$  with  $r_0/a$ , for both the flat punch and the sphere.

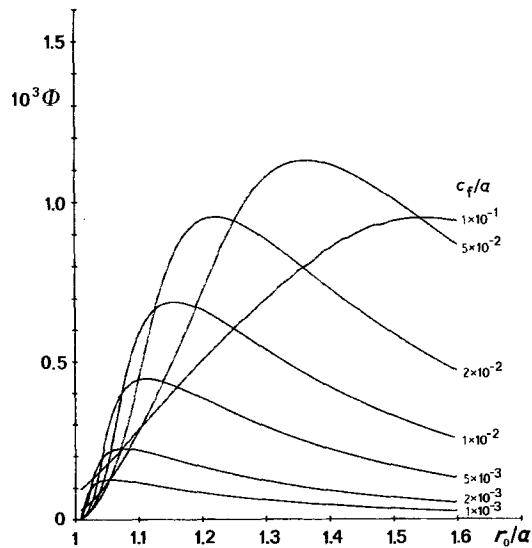


Figure 10 Flat punch ( $\nu = 0.22$ ). Strain energy release rate function  $\Phi$  for surface flaws of reduced length  $c_f/a$ , as a function of their relative location  $r_0/a$ .

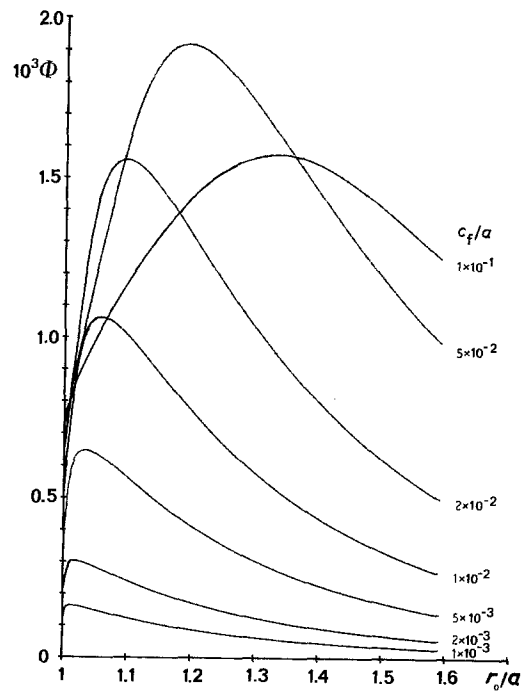


Figure 11 Spherical punch ( $\nu = 0.22$ ). Strain energy release rate function  $\Phi$  for surface flaws of reduced length  $c_f/a$ , as a function of their relative location  $r_0/a$ .

Thus for a given radius of contact and a surface with uniform distribution of flaw with the size  $c_f$ , the flaws situated at a distance  $r_0/a$  corresponding to the maximum of  $\Phi$  undergo the maximum stress intensity factor at the tip and will extend when the load is increased. Fig. 12 shows the displacement of this maximum with  $c_f/a$ : the starting radius  $r_0/a$  monotonically increases with  $c_f/a$ . Due to the steeper decrease of stresses, the starting radii are larger for the flat punch than for the sphere.

Curves at constant  $c_f/a$  in Figs. 10 and 11 represent vertical sections through the curves of

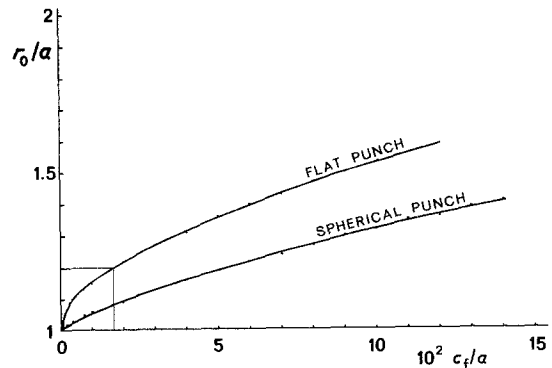


Figure 12 Starting radius  $r_0/a$  of the crack as a function of  $c_f/a$  ( $\nu = 0.22$ ).

Figs. 6 and 7, so that the maxima of the curves in Figs. 10 and 11 are the upper envelope of the curves in Figs. 6 and 7. (For clarity this envelope is not displayed.) It is thus possible to give a complete description of the phenomena by inspecting Figs. 6 and 7. Note that the ascending branch of the envelope is tangent to the unstable branches of the  $[\Phi(c_f/a)]_{r_0/a}$  curves, whereas the descending branch is tangent to the stable branches.

## 6. Critical load for the flat punch

Fig. 6 displays two maxima for  $r_0/a < 1.2$ ; from Fig. 12 this corresponds to  $c_f/a < 1.7 \times 10^{-2}$  (small flaws or large punches).

Let us first consider the case  $c_f/a < 1.7 \times 10^{-2}$ , and take for example  $c_f/a = 4 \times 10^{-3}$ . A vertical line from this point intersects the envelope, giving  $\Phi(c_f/a) = 3.7 \times 10^{-4}$  at  $r_0/a = 1.10$ . From Equation 8, the critical load for equilibrium is

$$P_c = 52 \left( \frac{\pi^3 E \gamma}{2(1 - \nu^2)} \right)^{1/2} a^{3/2} \quad (11)$$

From this unstable point, the curve  $r_0/a = 1.10$  must be followed. The crack extends at constant  $P_c$  and stops at  $c/a = 2.4 \times 10^{-2}$ . Increasing the load further (see Fig. 8), a second critical load  $P^*$  for the formed cone appears at  $c^*/a = 6.7 \times 10^{-2}$  with  $[\Phi(c^*/a)]_{1.10} = 2.7 \times 10^{-4}$ . Hence the critical load is

$$P^* = 61 \left( \frac{\pi^3 E \gamma}{2(1 - \nu^2)} \right)^{1/2} a^{3/2} \quad (12)$$

and the stable length of the cone is given by  $c/a = 1.47$ . The cone then stably extends when the load increases.  $P^*$  is 17% higher than  $P_c$  at  $c_f/a = 4 \times 10^{-3}$ ; it is 7% higher at  $c_f/a = 10^{-3}$  and 32% higher at  $c_f/a = 10^{-2}$ .

Consider now the case  $c_f/a > 1.7 \times 10^{-2}$ , say  $c_f/a = 3.1 \times 10^{-2}$ . The curves give  $\Phi(c_f/a) = 1.09 \times 10^{-3}$  at  $r_0/a = 1.30$  and the critical load is

$$P_c = 30 \left( \frac{\pi^3 E \gamma}{2(1 - \nu^2)} \right)^{1/2} a^{3/2} \quad (13)$$

The equilibrium is still unstable, but the crack propagates only to  $5 \times 10^{-2}$  and becomes stable.

Fig. 13 shows the variation of  $[\Phi(c_f/a)]^{-1/2}$  against  $c_f/a$  along the envelope. From Equation

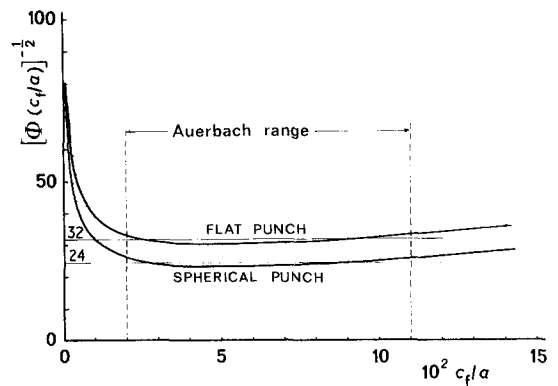


Figure 13 Variation of  $[\Phi(c_f/a)]^{-1/2}$  against  $c_f/a$  along the envelope of the curves Figs. 6 and 7. This quantity is proportional to  $P_c/a^{3/2}$ . The plateau represents the "Auerbach range".  $\nu = 0.22$ .

8 this quantity is proportional to  $P_c/a^{3/2}$ . For  $2 \times 10^{-2} < c_f/a < 1.1 \times 10^{-1}$ ,  $P_c$  becomes proportional to  $a^{3/2}$  and independent of the flaw size. The suddenness of the appearance of the crack and its size decrease as  $c_f/a$  increases. This is shown in Fig. 14 which gives the spontaneous crack extension at the critical load. (This critical load is  $P^*$  for  $c_f/a < 1.7 \times 10^{-2}$ .) It clearly appears that the flat part of Fig. 13 corresponds

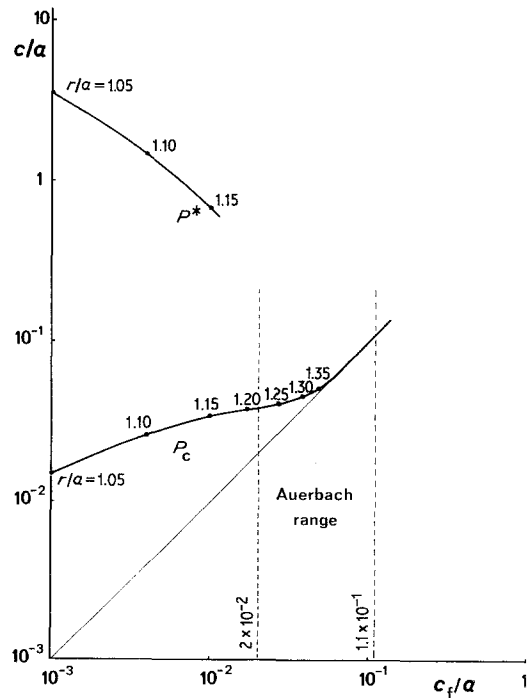


Figure 14 Flat punch ( $\nu = 0.22$ ). Equilibrium size of the crack under critical load  $P_c$  as a function of  $c_f/a$ . The computed starting of the crack is indicated.

to small cones or shallow rings connecting flaws well outside the radius of contact.

On the plateau (the ‘‘Auerbach range’’),  $[\Phi(c/a)]^{-1/2}$  takes the value 32 for  $\nu = 0.22$ , hence surface energy can be computed from the observed values  $B = P_c/a^{3/2}$  using the expression

$$\gamma = 6 \times 10^{-5} \frac{B^2}{E} \quad (14)$$

## 7. The case of the sphere: the Auerbach range

The case of the sphere is more complicated than that of the flat punch since the radius  $a$  increases with the load, so that  $c_f/a$  is no longer an initial datum of the problem. However, one has a supplementary equation, the Hertz law

$$a^3 = \frac{3}{4} \frac{1 - \nu^2}{E} kPR \quad (15)$$

with

$$k = 1 + \frac{1 - \nu'^2}{1 - \nu^2} \frac{E}{E'} \quad (16)$$

( $k = 1$  for a rigid indenter, and  $k = 2$  for indenter of the same material). Inserting this value in Equation 5, one has

$$G = \frac{16}{3\pi^3} \frac{P}{kR} [\Phi(c/a)]_{r_0/a} \quad (17)$$

and the critical load is

$$P_c = \frac{3\pi^3}{8[\Phi(c/a)]_{r_0/a}} k\gamma R \quad (18)$$

equivalent to Equation 8. At the instant of initiation,  $r_0$  and  $a$  are fixed (although still unknown) and the curve  $G/2\gamma$  against  $c_f/a$  for  $P = P_c$  has the same shape as the curve  $\Phi(c/a)$  in Fig. 7. If  $c_f/a$  is sufficiently small the equilibrium is unstable, and a large cone can be spontaneously formed at constant  $P_c$ ,  $r_0$  and  $a$ . The smaller value of  $c_f/a$ , the larger the cone.

At this stage the values of  $c_f/a$  and  $r_0/a$  are not yet known. Eliminating  $P_c$  between Equations 15 and 18 gives

$$[\Phi(c/a)]_{r_0/a} = \frac{9\pi^3(1 - \nu^2)}{32} \frac{\gamma R^2 k^2}{Ec_f^3} \left(\frac{c_f}{a}\right)^3 \quad (19)$$

The right-hand member gives a family of straight lines of slope 3 in Fig. 7, which are followed by increasing the load of constant  $c_f$ .

The values of  $c_f/a$  and  $r_0/a$  are determined by the intersection of these lines with the envelope of the  $[\Phi(c/a)]_{r_0/a}$  curves. As for the flat punch, this envelope corresponds to the maxima of the  $[\Phi(r_0/a)]_{c_f/a}$  curves of Fig. 11. It thus appears that  $r_0/a$  decreases as  $R$  increases, as observed by Hamilton and Rawson [26]. Fig. 13 gives the variation of  $P_c$  along this envelope. As for the flat punch, near the maximum of the envelope  $P_c$  becomes proportional to  $a^{3/2}$  (i.e. proportional to the radius  $R$  of the ball), and independent of the original flaw size for  $2.5 \times 10^{-2} < c_f/a < 10^{-1}$ , i.e. for  $0.3 < (\gamma R^2 k^2 / Ec_f^3) < 10$ . This is the Auerbach range. Taking  $[\Phi(c/a)]^{-1/2} = 24$  in Fig. 13 and defining  $B = P/a^{3/2}$ , the constant observed ratio, one has

$$\gamma = 1.07 \times 10^{-4} \frac{B^2}{E} \quad (20)$$

or using Equation 18

$$\frac{P_c}{R} = 6.7 \times 10^3 k\gamma = A \quad (21)$$

where  $A$  is the Auerbach constant. In this range near the maximum of the envelope only a shallow ring appears, as noted by Tillet [23] and Warren [6].

For very small  $c_f/a$  (large ball radius), the undiminishing stress field approximation for the critical load (Equation 10) gives

$$P_c = \frac{9}{(1 - 2\nu)^3} \left\{ \frac{2\pi^3(1 - \nu^2)}{E} \right\}^{1/2} \frac{\gamma^{3/2} R^2 k^2}{c_f^{3/2}} \left(\frac{r_0}{a}\right)^6 \quad (22)$$

as noted by Langitan and Lawn [21] (for  $r_0/a = 1$ ), and Wilshaw [22] (excepted for a factor 1.12). When  $c_f/a$  tends to zero,  $r_0/a$  tends to 1 (see Fig. 12) and  $P_c$  varies as  $R^2/c_f^{3/2}$ . For any value of  $\gamma R^2 k^2 / Ec_f^3$ ,  $\Phi(c/a)$  can be evaluated and then  $P_c$  by means of Equation 18. Fig. 15 displays the variation of  $P_c/\gamma R$  as a function of  $R/c_f^{3/2}$  and  $k = 1$  or 2, and for  $\gamma/E = 5 \times 10^{-11}$  m, a representative value for glass. For  $k = 1$ ,  $P_c/\gamma R$  can be considered as a constant for  $R/c_f^{3/2}$  varying between  $8 \times 10^4 \text{ m}^{-1/2}$  and  $4.5 \times 10^5 \text{ m}^{-1/2}$ , i.e. for  $R$  between 0.2 and 1.4 mm with  $c_f = 2 \mu\text{m}$ , or  $R$  between 2.5 and 16 mm with  $c_f = 10 \mu\text{m}$ . This range thus extends over a factor of 6.3 for  $R$ , and a factor 3.4 for  $c_f$ . Note that the largest observed ranges (Tillet [23], Powell and Tabor [32]) give a factor 8 for the radii.

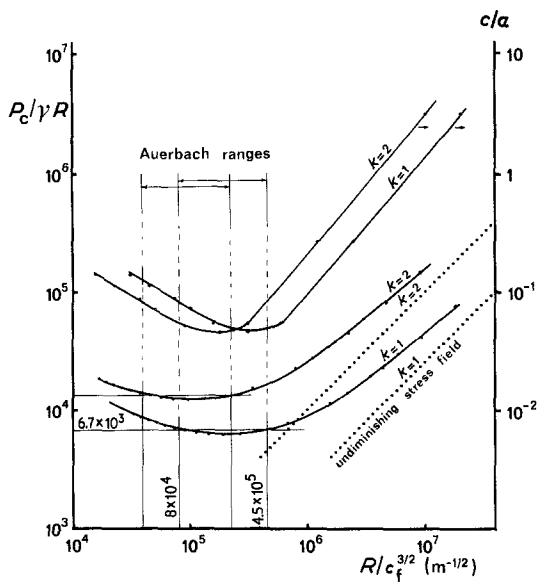


Figure 15 Spherical punch ( $\nu = 0.22$ ). Critical load and equilibrium size of the crack as a function of the radius of the ball, in reduced coordinates.  $k = 1$  is for a rigid sphere and  $k = 2$  for a sphere of the same material as the specimen.  $\gamma/E = 5 \times 10^{-11}$  m.

The limits of the Auerbach range can also be estimated by direct inspection of Fig. 7. The envelope of the  $\Phi(c/a)$  curves becomes nearly constant for  $0.3 < \gamma R^2 k^2 / E c_f^3 < 10$ ; hence the limits are given by

$$\left(\frac{0.3E}{\gamma k^2}\right)^{1/2} < \frac{R_u}{c_f^{3/2}} < \left(\frac{10E}{\gamma k^2}\right)^{1/2} \quad (23)$$

For large values of  $R/c_f^{3/2}$ ,  $P_c$  becomes progressively proportional to  $R^2$  (undiminishing stress field approximations). Such a behaviour from  $P_c \sim R$  to  $P_c \sim R^2$  was observed by several investigators [23, 26, 29, 33].

The extension  $c/a$  of the crack when stable equilibrium is reached is also given in Fig. 15. Only outside the Auerbach range (small  $c_f/a$ ), does a well-formed cone appear at  $P_c$ .

### 7.1. Discussion of the Auerbach "law"

Since the work of Roesler [34] the explanation of the Auerbach "law" has been the subject of dispute, for this law is an apparent violation of the Griffith criterion. The criterion for a flaw in equilibrium in a uniform stress field is

$$\sigma \sim \left(\frac{\gamma E}{c_f}\right)^{1/2} \quad (24)$$

Using the tensile stress at the edge of the contact,

$\sigma \sim P/a^2$  (Equation 1a), together with the Hertz law  $a^3 \sim PR/E$ , we obtain

$$P_c \sim \frac{\gamma^{3/2}}{E^{1/2} c_f^{3/2}} R^2 \quad (25)$$

This naive interpretation of the Griffith criterion (neglecting the stress distribution along the flaw) thus predicts  $P_c \sim R^2$ , not  $P_c \sim R$ . Conversely,  $P_c \sim R$  means  $\sigma \sim R^{-1/3}$ , a striking effect.

A first explanation based on flaw statistics was proposed by several authors [26, 29, 35, 36]: smaller indenters produce a smaller stressed surface area and have a lower probability of including large flaws, so that a larger load than that predicted by the  $R^2$  law must be applied. They all used the undiminishing stress field approximation, only valid for small  $c_f/a$ , i.e. large radii (where the Auerbach law does not hold!) and adjusted the two or three parameters of the flaw statistics to the experimental results. Furthermore one parameter appears to be ball-size dependent [37], and the three parameters obtained from the Hertzian tests differ from those obtained from bend tests [37, 38].

A second explanation was proposed by Lawn and co-workers [4, 15, 21] taking into account the stress distribution along the crack which they assume to start at  $r_0/a = 1$ . Unfortunately, they performed their calculation on a high value of  $\nu$  ( $\nu = 1/3$ ) that gives a hump on the  $\Phi(c/a)$  curve (when using Equation 2a), and they based their explanation on the existence of such a hump. They predict an Auerbach range extending over two powers of ten with well-formed cones in this range. However, as shown by Wilshaw [22] and Warren [6] such a hump does not exist for  $\nu = 0.25$  or disappear at  $\nu = 1/3$  for  $r/a > 1$ . Warren [6] pointed out the dramatic influence of  $\nu$  and  $r/a$ , and proposed to assign Auerbach's law to the maximum of  $\Phi(c/a)$  at  $c''/a$ , provided there are flaws of size larger than  $c''/a$ . His treatment does not hold for surface having flaws of unique length  $c_f$ ; in this case  $P_c$  goes through a minimum for  $c/a' = c''/a$  and then increases. Warren predicts also that there is no upper flaw-size limit for the validity of the Auerbach law [39], moreover his Auerbach constant depends on the observed  $r_0/a$ , and if  $r_0/a$  changes with  $R$ , Auerbach's law becomes impossible to explain with this theory.

The present analysis is based not on the  $\Phi(c/a)$  curves but on their envelope for various values

of  $r_0/a$ . It allows for the prediction of  $r_0/a$  at crack initiation, and an Auerbach range can be predicted even if all surface flaws have a constant size. The physical meaning of the Auerbach range is more obvious by considering that flat punch for which there is one less variable. At small  $c_f/a$  (large radii)  $P_c$  decreases when  $c_f/a$  increases as for any Griffith flaw of increasing length, but for large  $c_f/a$ ,  $P_c$  increases when  $c_f/a$  increases because the stresses at the crack tip become smaller and smaller. Between the two, there is a minimum in  $P_c$ . This minimum is a plateau for a balance between the two effects is found in this range by finding the appropriate value of  $r_0/a$  that gives the maximum value of  $G$ .

### 8. Stable propagation of the formed cone

For a given  $c_f$ , a well-formed cone can be obtained either instantaneously at the load  $P_c$  for a large punch, or from a ring crack by increasing  $P$  above  $P_c$ . In either case the formed cone of length  $c$  is in stable equilibrium, although this equilibrium can take very long to reach. Its length increases as  $P$  further increases. For a flat punch  $r_0/a$  remains constant during this stable growth, but for a sphere the value of  $r_0/a$  decreases as  $P$  increases; hence there is an uncertainty in computing  $\Phi(c/a)$ , as noted by Matzke and Warren [40], although they have shown by serial sectioning that the cone path is not very sensitive to the value of  $r_0/a$  at which it is created.

For well-formed cones with a base  $s$  much larger than  $a$ , Roesler [7] has shown by scaling laws that  $G$  could be written as

$$G = D \frac{P^2}{Es^3} \quad (26)$$

and gave for  $\nu = 0.25$  by a lengthy calculation  $D = 2.15 \times 10^{-2}$  as the upper bound. Equation 26 can be obtained by a more direct route (see Appendix) but gives  $D = 7.6 \times 10^{-2}$ . A calculation by the finite element method has been undertaken (to be published) which gives  $D = 5.7 \times 10^{-3}$  for  $\theta = 68^\circ$  and  $\nu = 0.22$ , a value 3.8 times lower than the Roesler one. This proportionality between  $s$  and  $P^{2/3}$  was well verified [7-11] for the fully developed cone. Note in passing that some experimenters used a sphere with a machined flat to give a constant area of

contact. In fact, in this geometry, the area of contact increases with load in a predictable manner [41, 42]. But fortunately Equation 26 is independent of the radius of contact.

Comparison of Equations 5 and 26 shows that at large  $c/a$ ,  $\Phi(c/a)$  should vary as

$$\Phi(c/a) = \frac{1.02 D}{\left(\frac{r}{a} + \frac{c}{a} \sin \theta\right)^3} \quad (27)$$

with a slope of the curves  $y = \log \Phi$  against  $x = \log(c/a)$  given by

$$\frac{dy}{dx} = -3 \frac{\frac{c}{a} \sin \theta}{\frac{r}{a} + \frac{c}{a} \sin \theta} \quad (28)$$

Equation 27 with the Roesler  $D$  value is compared to the numerical integration of Equation 6 in Figs. 6 and 7. The terminal slope  $m = -1.7$  for  $r_0/a = 1.6$  is still different from the value  $m = -2.56$  derived from Equation 28, but this result is much better than the slope  $m = -0.8$  obtained when using Equation 2a instead of Equation 2b. This slight discrepancy can arise either from a lack of precision in numerical computation at large  $c/a$ , or from the fact that the analysis uses the stress tensor of the uncracked half-space. Certainly stresses and stress trajectories are modified in the presence of a well-formed cone, and a detailed comparison with calculation by the finite element method will be of interest.

### 9. Influence of the Poisson ratio

As pointed out by Warren [6] the curves  $\Phi(c/a)$  are very sensitive to the Poisson ratio. For example, Figs. 16 and 17 show the curves  $\Phi(c/a)$  for various values of  $\nu$  and three of  $r_0/a$ , for the flat punch and the sphere. So, a large error in the Auerbach constant can arise if the proper value of  $\nu$  is not used. For  $\nu = 1/3$ , Langitan and Lawn [21] gave

$$A = 2 \times 10^5 k \gamma \quad (29)$$

(with  $k$  defined by our Equation 16). The difference of a factor 30 compared with Equation 21 arises both from the choice of  $\nu = 1/3$  and from the fact that they used the minimum of  $\Phi(c/a)$ . When applied to glass their formula gives a fracture energy too low by an order of

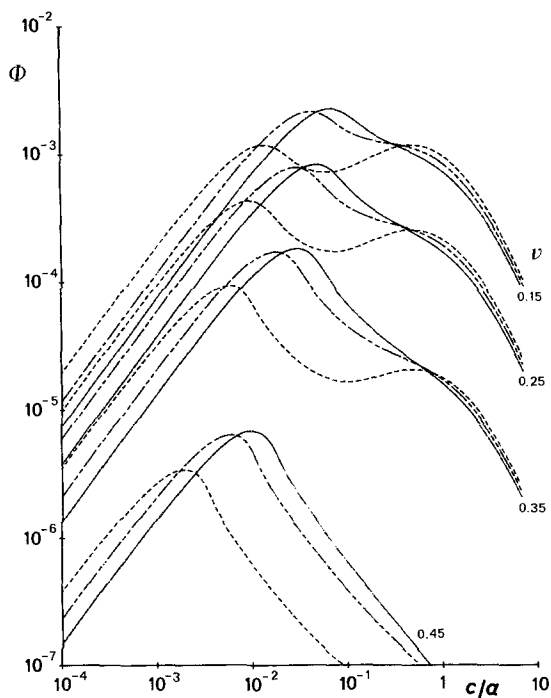


Figure 16 Flat punch. Strain energy rate function  $\Phi(c/a)$  for various Poisson ratios and starting radii. (---)  $r_0/a = 1.10$ ; (-----) 1.25; (—) 1.40.

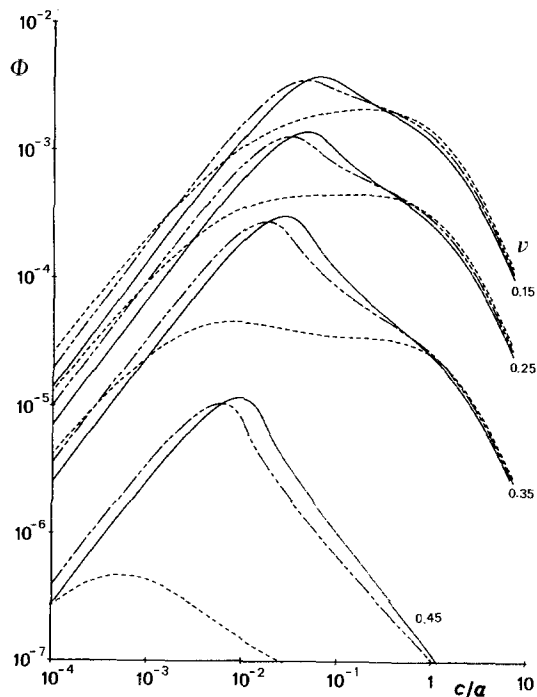


Figure 17 Spherical punch. Strain energy rate function  $\Phi(c/a)$  for various Poisson ratios and starting radii. (---)  $r_0/a = 1.00$ ; (-----) 1.10; (—) 1.20.

magnitude, as noted by Nadeau [30] and Nadeau and Rao [12].

## 10. Experiments

### 10.1. Procedure

Tests were made on optical glass plates (borosilicate glass) measuring 50 mm  $\times$  50 mm  $\times$  25.4 mm. Elastic properties of the glass measured by ultrasonic methods were  $\nu = 0.22 \pm 0.02$  and  $E = 8.0 \times 10^{10} \pm 0.1 \times 10^{10}$  Pa.

Before indentation, surfaces were abraded in two perpendicular directions using Nos. 400, 600, 1000 and 1200 SiC abrasive paper or 7  $\mu$ m diamond paste. Samples were stored in air in the laboratory, sometimes for days, before testing. No attempts were made to "freeze in" the state of the specimens, by immersing them in liquid nitrogen before testing to avoid the ageing of abrasions as suggested by Mould [43], for the authors were unaware of his work at that time. This negligence can explain a large part of the scatter of experimental results. The depth of microcracks was not measured, but following Langitan and Lawn [21] was taken as half the nominal particle size, i.e.  $c_f = 19 \mu$ m for SiC 400,  $c_f = 10 \mu$ m for SiC 1000 and 1200, and  $c_f \approx 3 \mu$ m for the diamond paste. Note however that other authors gave smaller estimations: Mould and Southwick [44] estimated the depth of damage to 5  $\mu$ m for 600 grit emery, and to 10  $\mu$ m for 320 grit emery, whereas Pavelchek and Doremus [45] proposed a median crack length of 6  $\mu$ m for 400 grit SiC paper.

The elastic properties of the steel indenters were  $\nu = 0.33$  and  $E = 2.1 \times 10^{11}$  Pa, so that  $k = 1.35$ . The radii of the flat punches were 0.05, 0.1, 0.25, 0.5, 1 and 2.5 mm; the radii of the spheres were 0.79, 2.37, 3.17, 5.15, 7.53, 12.7, 15.87, 24.61 and 37.51 mm.

The specimens were indented at 20°C on an Instron testing machine at the minimum speed (50  $\mu$ m  $\text{min}^{-1}$ ). The area of contact and the crack were observed through a prism and measured with a micrometer (Fig. 18). The machine was stopped as soon as an event was detected, the load  $P_c$  noted\*, and measurements made after 3 min. Depending on the indenter size and on the abrasion, two events could be observed: either the sudden apparition of a cone, or a small light corresponding to a growing flaw. In the

\*This load is an apparent critical load, and its meaning will be discussed in Section 11.

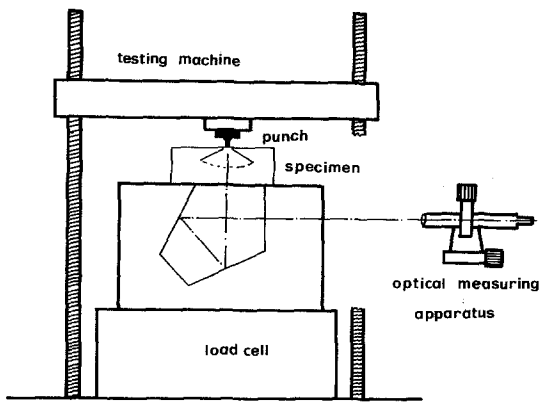


Figure 18 Schematic view of the apparatus.

either case, the crack continued to propagate, but very slowly, when the machine was stopped, and a small load relaxation could be observed at fixed machine displacement. In the second case, in order to easily measure the radius of the crack, the load was slightly increased so that this starting crack could gently run around the contact area. About twenty indentations were made for every indenter and every abrasion. Experiments were performed in the laboratory atmosphere at 20°C and a relative humidity of about 40%.

### 10.2. The starting radius of the crack

The ratios of the observed crack radii to the radii of contact are given in Figs. 19 and 20. For the two kinds of punches,  $r_0/a$  decreased as the radius of contact increased; moreover the starting radii were larger for the flat punches than for the spherical punches. All these three results are in

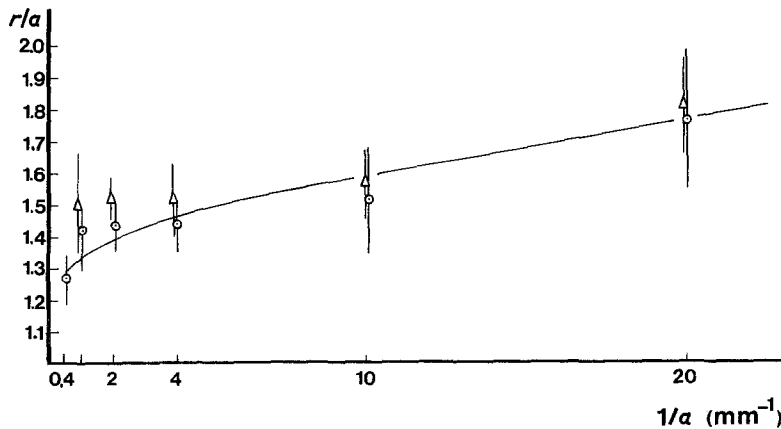


Figure 19 Flat punches. Starting radius of the crack against the reciprocal of the punch radius, for two abrasions: ( $\circ$ ) SiC 1000, ( $\Delta$ ) SiC 400.

agreement with the theory of a maximum of  $G$  for flaws not too close to the contact circle.

However, when compared to theoretical values, these starting radii appear higher. This means that other phenomena such as flaw statistics and interfacial shear stresses cannot be neglected.

### 10.3. Critical load for the flat punch

The results given in Fig. 21 can be compared to the theoretical curve in Fig. 13.  $P_c$  becomes proportional to  $a^{3/2}$  and independent of  $c_f$  for sufficiently small radii, the limiting radius increasing with  $c_f$ . With the estimated  $c_f$ , the limiting observed values are  $c_f/a = 8 \times 10^{-2}$  for SiC 400,  $4 \times 10^{-2}$  for SiC 1000 and  $2 \times 10^{-2}$  for diamond paste, compared to the predicted value  $c_f/a = 2 \times 10^{-2}$ .

In the experimental range  $1.2 \times 10^{-3} < c_f/a < 4 \times 10^{-1}$ , an intermediate stable equilibrium should have been detected for  $c_f/a < 2.6 \times 10^{-2}$ . Such a stepwise process was not observed. Two reasons can be invoked: the equilibrium values of  $c/a$  are small and difficult to detect, and the load continuously increases so that  $P^*$  can be reached before the equilibrium crack has finished its propagation round the indenter.

The cones formed had an angle  $\theta \approx 68^\circ$ , and the length of the crack approximately given by

$$c = \left( \frac{s}{2} - r \right) \frac{1}{\sin \theta} \quad (30)$$

is displayed in Fig. 22. This figure shows that the spontaneous extension of the cone decreases, and then disappears in the plateau regime where

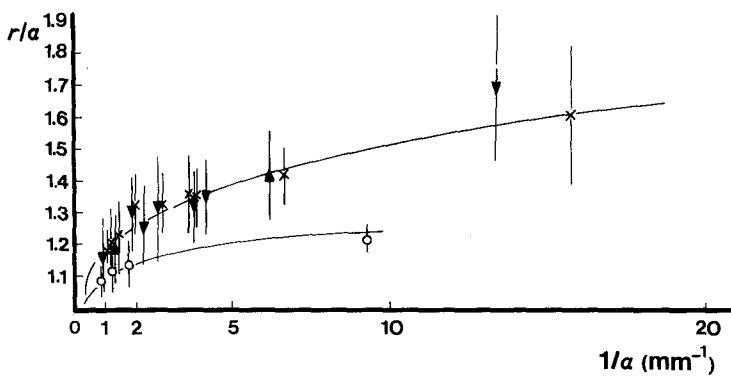


Figure 20 Spherical punches. Starting radius of the crack against the reciprocal of the contact radius, for three abrasions: (○) diamond 6 μm, (▼) SiC 1000, (×) SiC 400.

$P_c$  becomes proportional to  $a^{3/2}$ , in agreement with the theory.

Taking  $B = P_c/a^{3/2} = 75 \times 10^6 \text{ N m}^{-3/2}$  from Fig. 21, Equation 14 gives  $\gamma = 4.2 \text{ J m}^{-2}$ . Fig. 23 shows the distribution of  $\gamma$  when using the results given by the two punches  $a = 0.25$  and  $0.1 \text{ mm}$  at various abrasions (except diamond paste for  $a = 0.25 \text{ mm}$ ) with  $\Phi = 10^{-3}$ .

#### 10.4. Critical load for the sphere

Measurements of the radii of contact just before fracture give values larger than the calculated ones, by about 16%. This discrepancy, often quoted in Hertzian indentation [23, 39, 46–48], may arise from the roughness of the glass. The elastic contact of a smooth sphere with a nominally flat random rough surface has been considered in a number of papers [49–53]: at high loads the behaviour is Hertzian, but at low loads the deformation is almost entirely confined to asperities, the maximum pressure is much less

than the Hertz value, and contact spreads over an area much greater than the Hertz circle. Fig. 24 shows the radius of contact against load for SiC 1000 abrasion and three different ball radii: the radii of contact are larger than the calculated ones, especially at low loads. From Greenwood and Tripp [49], high loads begin for

$$T = \frac{2(1 - \nu^2) kP}{\sigma E(2R\sigma)^{1/2}} > 200 \quad (31)$$

where  $\sigma$  is the standard deviation of the height distribution. Attempts have been done to measure  $\sigma$  with a Talysurf but “high load” limits computed were too low by an order of magnitude, presumably because the diamond could not reach the bottom of roughness, giving thus a  $\sigma$  too low. As noted by Johnson *et al.* [27] the effect of surface roughness is to reduce the maximum value of the tensile stress and to increase the radius at which it occurs. This effect is qualitatively similar to that of interfacial friction.

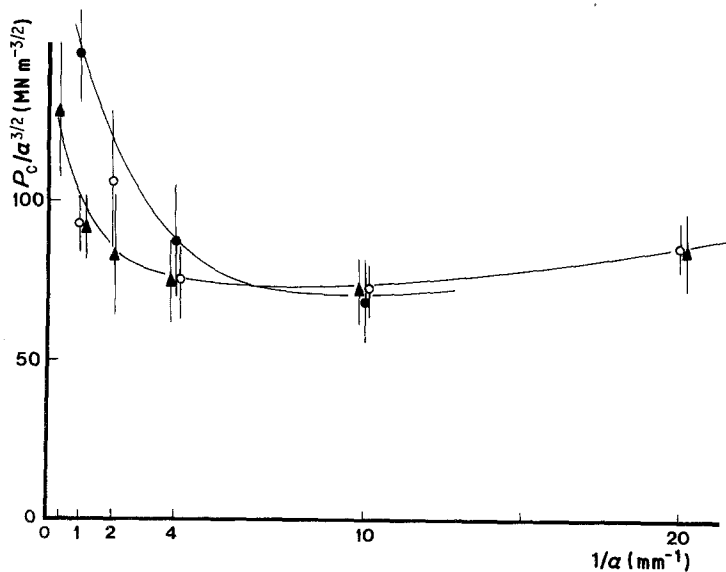


Figure 21 Flat punches. Apparent critical load against the reciprocal of the punch radius. The plateau corresponds to the “Auerbach range”. Abrasion (●) diamond 6 μm, (○) SiC 1000, (▲) SiC 400.

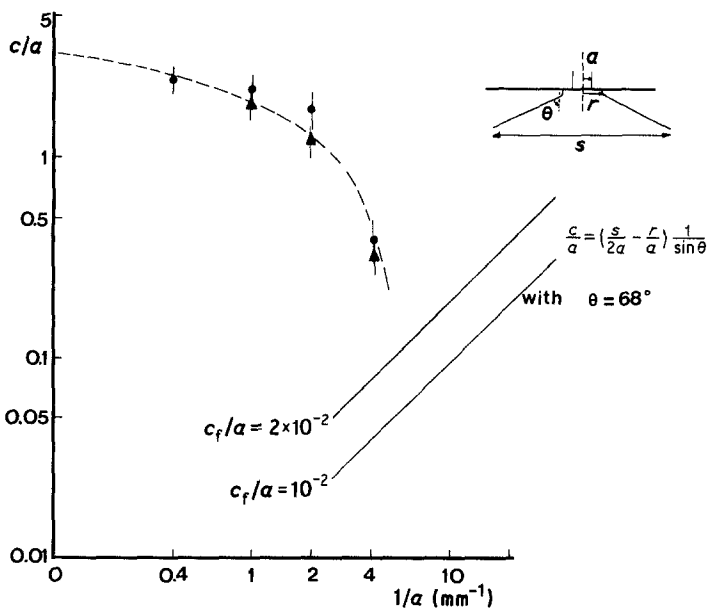


Figure 22 Flat punches. Extension of the cone after 3 min under the apparent critical load, for various punch radii and abrasions: (●) SiC 1000, (▲) SiC 400.

Fig. 25 shows  $P_c/R$  against  $R$ . For SiC 400, 1000, and 1200 an Auerbach range is observed. In this range, the critical load corresponds to a surface crack slowly running round the contact area. In the case of abrasion with diamond paste no Auerbach range is found, and a well-formed cone suddenly appears at  $P_c$ . With the Auerbach constant  $A = 50 \times 10^3 \text{ Nm}^{-1}$ , Equation 21 gives  $\gamma = 5.5 \text{ Jm}^{-2}$ . This equation involves a theoretical Hertz radius, but if instead the observed radii of contact are used, and  $P_c/a^{3/2}$  plotted against  $1/a$  (Fig. 26) as for the flat punch, the observed plateau gives  $P_c/a^{3/2} =$

$B = 6 \times 10^7 \text{ Nm}^{-3/2}$ , and  $\gamma$  computed from Equation 20 is  $4.8 \text{ Jm}^{-2}$  closer to the value obtained for the flat punch ( $\gamma = 4.2 \text{ Jm}^{-2}$ ). Fig. 27 shows the distribution of  $\gamma$  when using the results given by five ball radii in the Auerbach range, with  $\Phi = 1.8 \times 10^{-3}$  as the maximum of the envelope; the mean value is  $\gamma = 4.6 \text{ Jm}^{-2}$ .

However, the limiting values  $R_u$  for the Auerbach range are not in agreement with the theory. Inserting  $\gamma = 4.5 \text{ Jm}^{-2}$  in Equation 23 one would have  $R_u = 1.6 \text{ mm}$  for  $c_f = 3 \mu\text{m}$ ,  $R_u = 9.9 \text{ mm}$  for  $c_f = 10 \mu\text{m}$ , and  $R_u = 26 \text{ mm}$  for  $c_f = 19 \mu\text{m}$ . The observed values of  $R_u$  are larger for SiC papers and smaller for diamond paste.

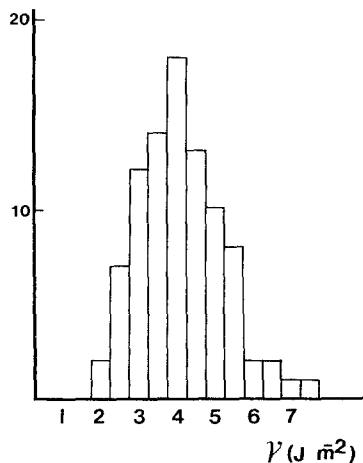


Figure 23 Flat punches. Histogram of apparent surface energy computed from Equation 8 with  $\Phi = 10^{-3}$  (Auerbach range). Punch radii 0.25 and 0.1 mm;  $\nu = 0.22$ ;  $E = 8 \times 10^{10} \text{ Pa}$ ; mean  $\gamma = 4.06 \text{ Jm}^{-2}$ .

### 10.5. The well-formed cone

Well-formed cones are observed both with flat punches and spheres, either suddenly at  $P_c$  for small  $c_f/a$  or by increasing the load after initiation of a circular ring. The results are given in Fig. 28 for a 3 min contact under load. The relation between  $s$  and  $P^{2/3}$  is well verified and is independent of the shape of the indenter and the abrasion. Application of the Griffith relation  $G = 2\gamma$  with  $G$  given by Equation 26 and with the Roesler value  $D = 2.15 \times 10^{-2}$  leads to  $2.5 < \gamma < 8 \text{ Jm}^{-2}$ , whereas the rough calculation given in the Appendix (with  $\nu = 0.22$  and  $\theta = 68^\circ$ ) leads to  $8 < \gamma < 16 \text{ Jm}^{-2}$ , values certainly too high. On the other hand, calibration by the finite element method gives

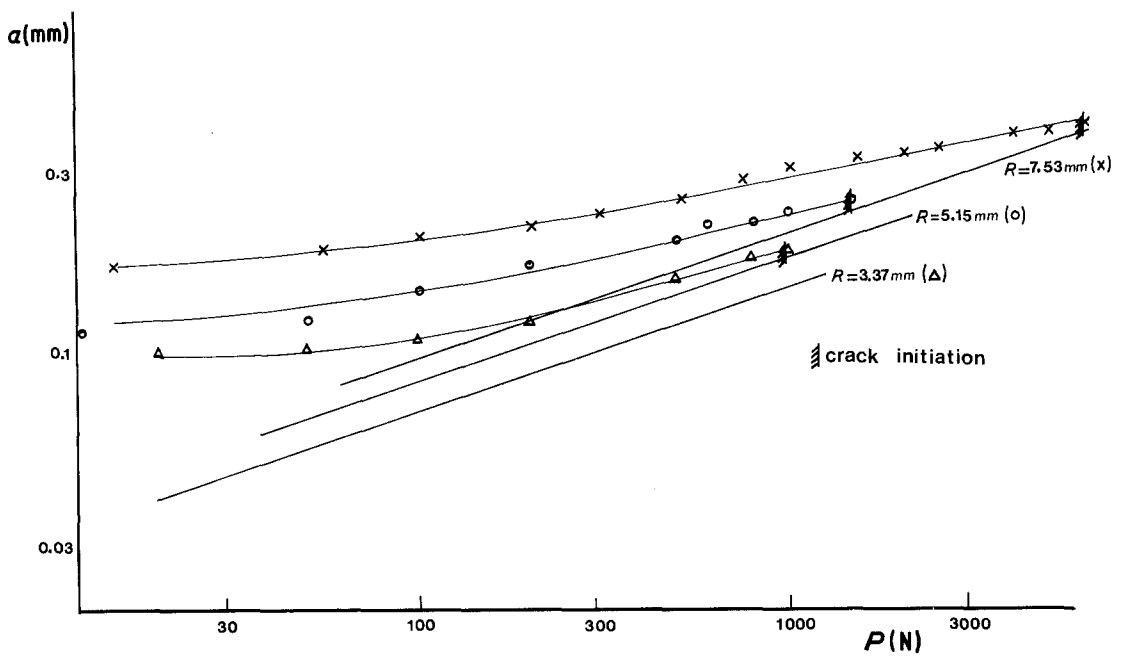


Figure 24 Spherical punches. Observed radius of contact against load for three ball radii, and abrasion with SiC 1000. At low loads radii of contact depart from the Hertz law (Equation 15) illustrated by the labelled straight lines:  $k = 1.356$ ,  $E = 8 \times 10^{10} \text{ Pa}$ ,  $\nu = 0.22$ .

$0.65 < \gamma < 2 \text{ J m}^{-2}$ ; these low values are not unrealistic, as discussed in Section 11.

After 3 min the crack is not yet in equilibrium and continues to grow for hours. After one hour

the value of  $\gamma$  given by the Roesler formula is about  $1.25 \text{ J m}^{-2}$ , whereas it is about  $0.32 \text{ J m}^{-2}$  by the finite element method. Such kinetic effects in Hertzian fracture have been observed by

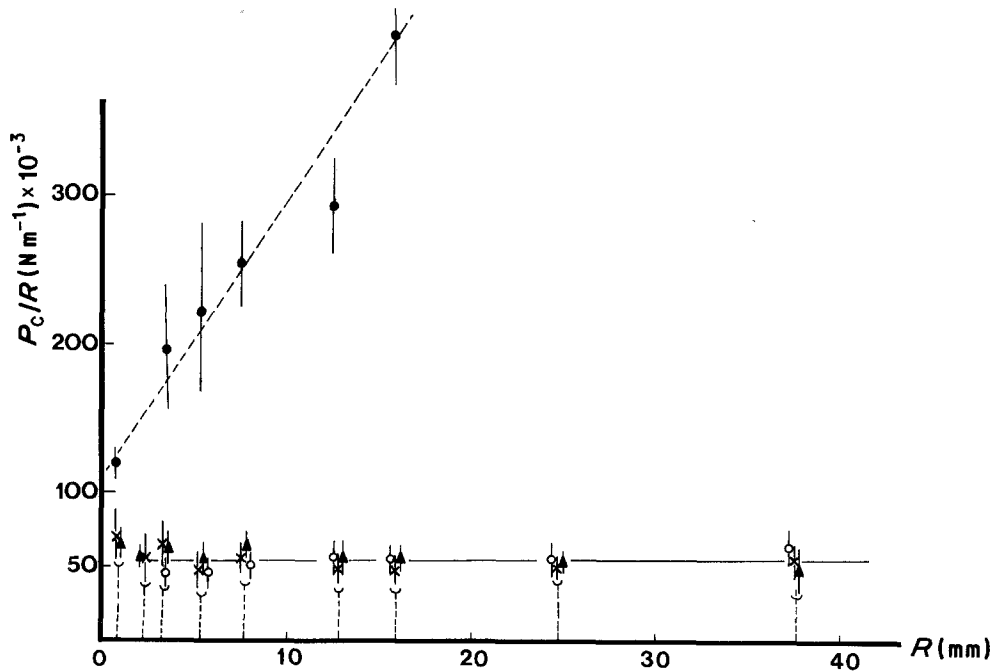


Figure 25 Spherical punches. Apparent critical load against ball radius for four abrasion types. The Auerbach law is obeyed with SiC but not with diamond paste. With the Auerbach constant  $A = 50 \times 10^3 \text{ N m}^{-1}$ , Equation 21 gives  $\gamma = 5.5 \text{ J m}^{-2}$ . Abrasion (●) diamond  $6 \mu\text{m}$ , (○) SiC 1200, (×) SiC 1000, (▲) SiC 400.

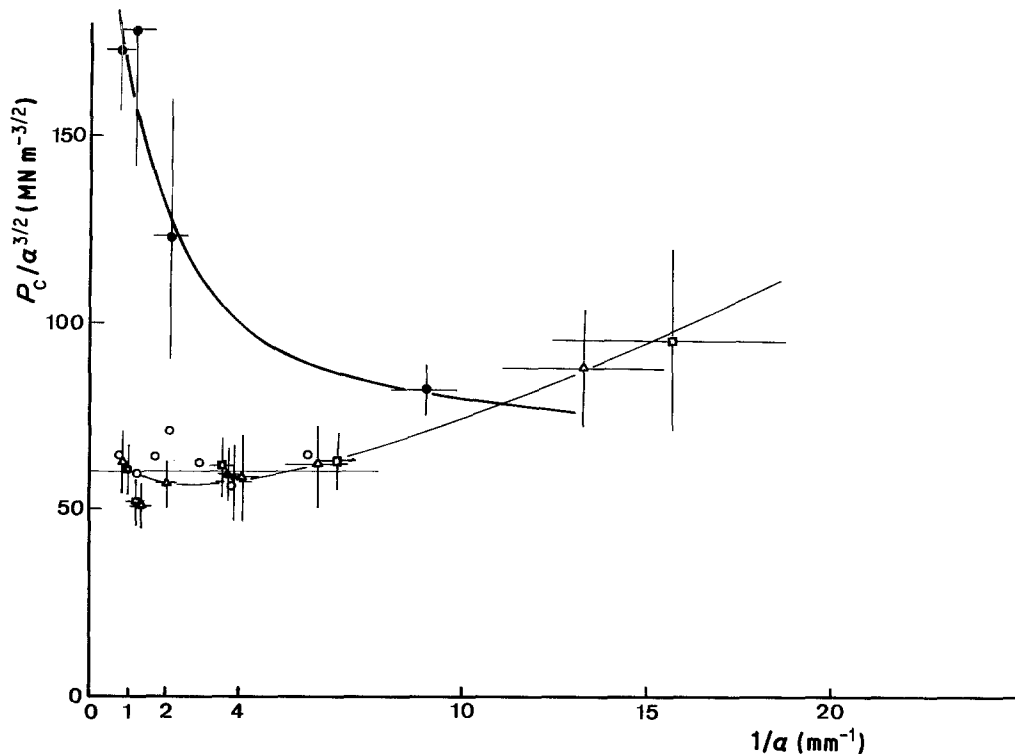


Figure 26 Spherical punches. Apparent critical load against the reciprocals of observed contact radii, for four abrasion types. From the Auerbach range observed with SiC, Equation 20 gives  $\gamma = 4.8 \text{ J m}^{-2}$ . Abrasion (●) diamond  $6 \mu\text{m}$ , (○) SiC 1200, (△) SiC 1000, (□) SiC 400.

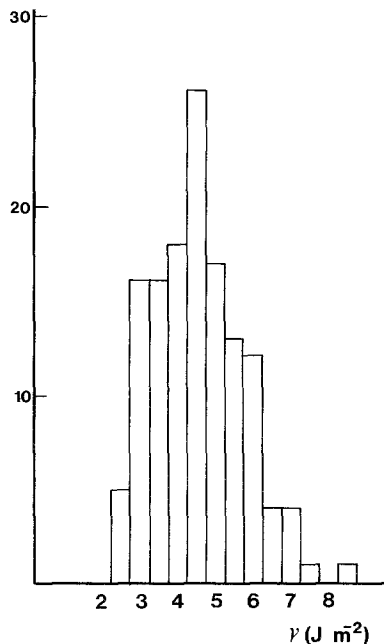


Figure 27 Spherical punches. Histogram of apparent surface energy computed from Equation 8 with  $\Phi = 1.8 \times 10^{-3}$  (Auerbach range). Punch radii 3.17, 5.15, 7.58, 12.7 and 15.87 mm;  $\nu = 0.22$ ;  $E = 8 \times 10^{10} \text{ Pa}$ ; mean  $\gamma = 4.6 \text{ J m}^{-2}$ .

Roesler [7], Tillet [23], Culf [8], Argon *et al.* [24], Langitan and Lawn [54], Mikosza and Lawn [55], Nadeau and Rao [12], Lawn [56], Swain and Lawn [10], and Conrad *et al.* [28]. In particular Roesler [7] noted that “twenty seconds after loading the value of  $\gamma$  is twice the 15-minute value. After the load has been on for several days the value of  $\gamma$  is half the 15-minute value”. This slow crack growth is discussed below.

## 11. Subcritical crack growth

Hitherto, we have applied the Griffith criterion without precaution, and we have to discuss the significance of the  $\gamma$  values so obtained. This problem of intrinsic surface energy, fracture toughness and subcritical crack growth is discussed in more detail by Maugis [57], and only a brief account is given here. The analysis is based on the model proposed by Maugis and Barquins [58, 59] for the kinetics of crack propagation between rigid punches and viscoelastic solids (e.g. polyurethane).

Thermodynamics shows that a crack is in equilibrium if  $G = 2\gamma$  (the Griffith criterion) where  $\gamma$  is the intrinsic surface energy. This

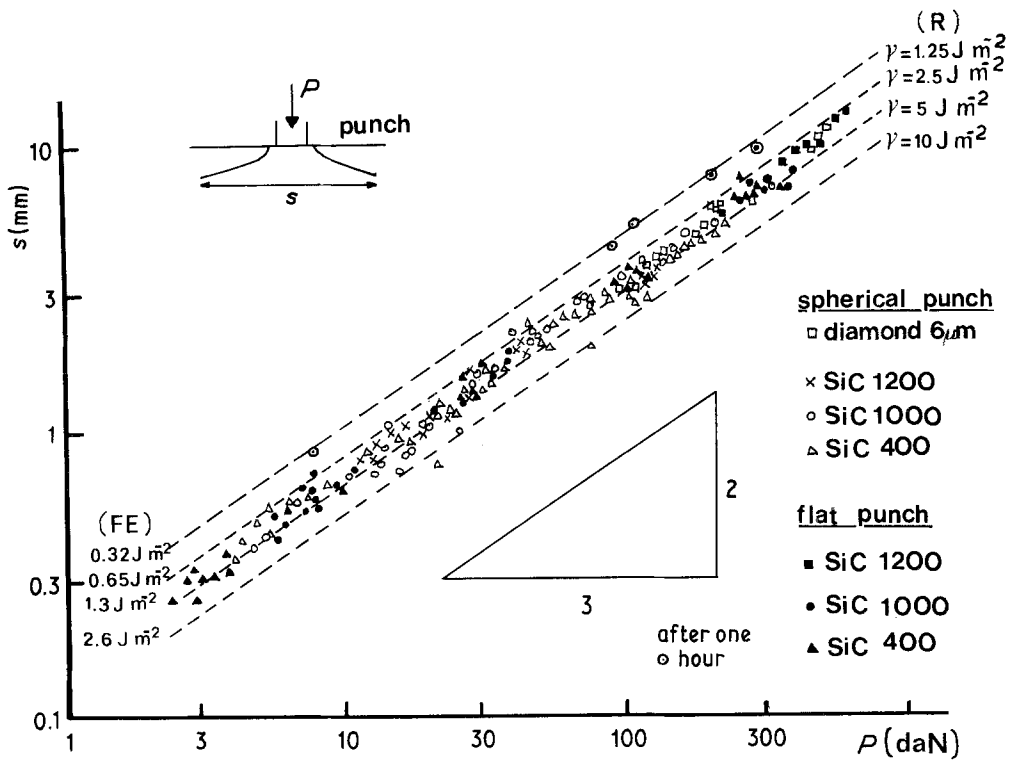


Figure 28 Well-formed cones. Diameter of the base of the cone against load after 3 or 60 min contact. Surface energy estimated from Roesler approximation (R) and from finite-element calculation (FE).

equilibrium is stable at fixed load if  $(\partial G/\partial c)_P < 0$  and unstable if  $(\partial G/\partial c)_P > 0$ . If  $G > 2\gamma$  the crack advances and if  $G < 2\gamma$  it recedes. Such equilibrium and crack recession have been observed at the glass-polyurethane interface. The Dupré energy of adhesion  $w$  (that replaces  $2\gamma$  at an interface) deduced from equilibrium cracks was about  $50 \text{ mJ m}^{-2}$ .

$(G - 2\gamma)$  is the force applied per unit length of crack. In a purely elastic solid, a crack subjected to a constant force  $(G - 2\gamma) > 0$  continuously accelerates. In a real solid, dissipation occurs at the crack tip (due to viscoelasticity or internal friction) and the crack takes a constant velocity  $v$ . Maugis and Barguins [58, 59] have proposed the equation

$$G - 2\gamma = 2\gamma\alpha(T)\phi(v) \quad (32)$$

where the multiplicative factor  $\gamma$  on the right-hand side means that losses at the crack tip are proportional to the intrinsic surface energy. (Losses only arise if the interface itself is capable of withstanding stress, as noted by Gent and Schultz [60] and Andrews and Kinloch [61] in their studies of adhesion failure.) This equation is astonishingly well verified for glass-

polyurethane with  $\phi(v) \sim v^{0.6}$  over about five powers of ten in velocity. In particular, the whole curve  $\log G$  against  $\log v$  is translated towards lower values of  $G$  in the presence of water vapour, even at high  $G$  values ( $G \gg w$ ). Maugis [62] has pointed out that above a critical velocity  $v_c$ , corresponding to a critical strain energy release rate  $G_c$ , the energy losses at the crack tip can decrease, but that the branch with a slope  $d\phi/dv$  negative cannot be observed, so that the speed jumps (with acoustic emission) to a value some orders of magnitude higher on a second stable branch most probably related to energy losses by radiation near the Rayleigh velocity. Fig. 29 shows the superposition of a curve of brittle fracture (with dynamic effects) and a curve for viscoelastic losses or internal friction. The condition of stable or unstable crack propagation defined by the sign of  $d\phi/dv$  is related to the thermodynamics of irreversible processes [57] and must not be confused with the condition of stable or unstable equilibrium defined by the sign of  $\partial G/\partial c$ . In this model one has

$$G < 2\gamma \quad \text{crack closure}$$

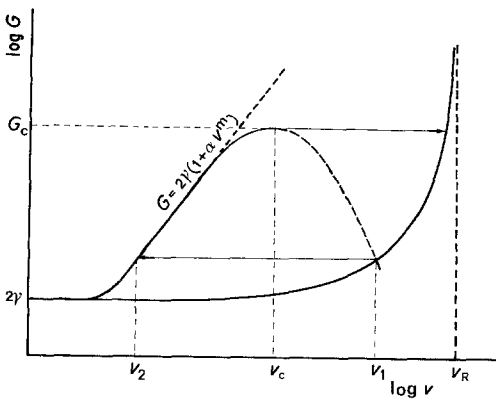


Figure 29 Superposition of a curve for brittle fracture (with dynamic effects) and a curve for viscoelastic losses or internal friction. Subcritical crack growth corresponds to  $v < v_c$ . The negative branch cannot be observed and a jump in velocity occurs, with acoustic emission, at  $G_c$ . When a mean velocity between  $v_c$  and  $v_1$  is imposed, stick-slip motions occurs.

- $G > 2\gamma$  crack advance  
 $2\gamma < G < G_c$  subcritical crack growth  
 $G > G_c$  catastrophic crack propagation

If  $v_c$  is small, the crack growth is not apparent and the condition  $G = G_c$  for crack velocity discontinuity and catastrophic failure can easily be confused with the condition  $G = 2\gamma$  for crack equilibrium by writing  $G_c = 2\gamma_f$  where  $\gamma_f$  is a "fracture surface energy" (for glass-polyurethane  $G_c \simeq 10^3 w$ ). However if so, subcritical crack growth in a vacuum becomes incomprehensible, and stress corrosion must be invoked to explain the increase in crack velocity with humidity. This proposed model can also explain embrittlement effects and stick-slip crack motion when a mean velocity is imposed in the negative branch range [57].

In this view, the static fatigue limit  $K_0$  of glass corresponds to an equilibrium crack and gives the intrinsic surface energy. For soda-lime glass in a vacuum or in dry air this static fatigue limit is about  $K_0 = 0.50 \text{ MPa m}^{1/2}$  [63], i.e. for plane stress (DCB, CT or DT specimens)  $\gamma_0 = 1.8 \text{ J m}^{-2}$ , whereas the critical stress intensity factor is  $K_{Ic} = 0.76 \text{ MPa m}^{1/2}$ , i.e.  $\gamma_f = 3.9 \text{ J m}^{-2}$  [64, 65]. In the presence of humidity the whole  $\log v - \log K_1$  curve is shifted towards lower values of  $K_1$  (Fig. 30), but this phenomenon is obscured by the limitation of the rate of water transport to the crack tip (Region II), and one returns to the vacuum value (Region III) at high velocity. Literature data

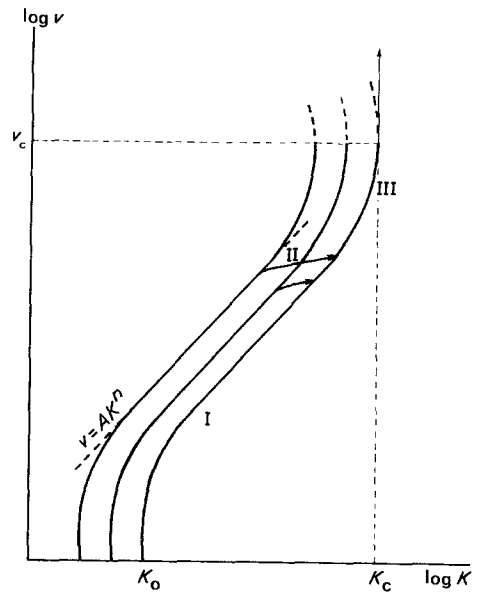


Figure 30  $v(K_1)$  curves. Lowering the intrinsic surface energy shifts the whole curve to lower  $K$  values.

give  $K_0 = 0.25 \text{ MPa m}^{1/2}$ , i.e.  $\gamma = 0.45 \text{ J m}^{-2}$ , for soda-lime [66, 67] or borosilicate in water [66].

Let us return to Hertzian fracture (Fig. 9) and assume for simplicity that  $G_c/2\gamma = 10$  in moist air. (This ratio is in agreement with the fact known since the work of Holland and Turner [68] that the endurance limit is about one-third of the instantaneous tensile strength.) Starting with an initial flaw  $c_f < c''$ , the load is increased at constant rate until  $G = 2\gamma$  (Point A). At this point the flaw is in unstable equilibrium and begins to grow, with  $G$  increasing as the crack length increases, but the crack velocity near  $G = 2\gamma$  is so low that this growth is not apparent; the applied load is allowed to increase, missing  $P_c$ , until something happens. An event can be detected, and the machine stopped, when the crack velocity reaches (say)  $10^{-3} \text{ m sec}^{-1}$  (Point B). But subcritical crack growth curves show that such a velocity corresponds to  $G \simeq G_c$ . The lower the loading rate, the larger the time allowed for the flaw to grow and reach high  $G$  values and the lower the apparent critical load, as shown by Langitan and Lawn [54], Swain *et al.* [69] and Conrad *et al.* [28]. From Points B to C the crack velocity sharply increases and then decreases. At Point C a ring has been formed quasi-instantaneously, but the crack continues to grow more and more slowly for hours towards the equilibrium cone at Point D. If the starting flaw

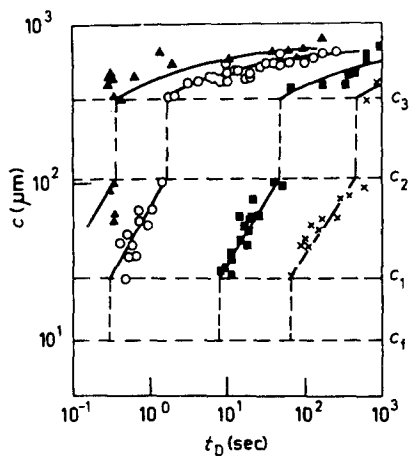


Figure 31 Cone crack length  $c$  as a function of indentation time  $t_D$  for four test environments: ( $\blacktriangle$ ) water, ( $\circ$ ) air, ( $\blacksquare$ ) toluene, ( $\times$ ) silicone oil. All data for  $P_e = 65$  kg. Note discontinuities in growth across “forbidden” gaps, and the similarity in the shapes of curves for different environments (after Mikosza and Lawn [55]).

$c'_f$  is smaller, when the machine is stopped at Point B' a large cone is instantaneously formed at Point C' with a crack velocity reaching catastrophic speed at the maximum of  $G$ . On the other hand, if the machine is stopped at point B'', the crack grows subcritically to the length  $c_f$  at Point B, where its velocity becomes apparent and then a ring abruptly appears at Point C. The time needed for the crack growth between B'' and B looks like an *incubation time*, as observed by others [70, 71]. If only fast propagation is considered, the behaviour closely resembles the theoretical one, but with  $\gamma$  replaced by a value near  $\gamma_f$ . This could justify the Irwin–Orowan concept of fracture surface energy. Indeed, the values of  $\gamma$  obtained in Section 10 ( $4.2. \text{ J m}^{-2}$  for flat punches,  $4.48 \text{ J m}^{-2}$  for spheres) approach the value  $\gamma_f = 5.2$  to  $5.8 \text{ J m}^{-2}$  derived from  $K_{Ic} = 0.85$  to  $0.90 \text{ MPa m}^{1/2}$  for borosilicate [65, 72].

We can now interpret the results of Mikosza and Lawn [55] and Lawn [56]. They applied a constant load  $P_e$  to a ball, and measured the crack length by sectioning and etching after various times of load application. They observed a slow crack growth followed by a sudden crack growth giving a forbidden gap in crack length, and then slow crack growth with decreasing speed (Fig. 31). At low  $P_e$  values this forbidden gap disappeared, whereas at high  $P_e$  values the first stage of slow crack growth disappeared (Fig. 32). These results were interpreted as a

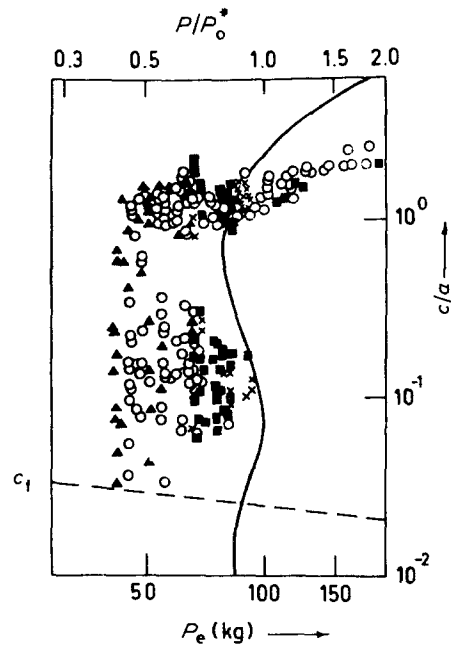


Figure 32 Cone crack length  $c$  (normalized to contact radius  $a$ ) as a function of indenter load  $P_e$ . Data points for tests in ( $\blacktriangle$ ) water, ( $\circ$ ) air, ( $\blacksquare$ ) toluene, and ( $\times$ ) silicone oil (after Mikosza and Lawn [55]).

tunnelling through the hump from the  $c_1$  to the  $c_2$  branch, and as a proof of the  $G$  against  $c/a$  curves with two maxima and a hump. This was puzzling, for it has been known since the work of Warren [6] that there is only one maximum for  $\nu = 0.25$ . Their results can be clearly understood with the help of Fig. 9. The first stage of slow crack growth corresponds to B''B, the apparent forbidden gap to BC, and the slowing crack to CD. At lower  $P_e$  the apparent forbidden gap disappears because the maximum velocity is low; at higher  $P_e$  the first stage of slow crack growth disappears. The increase in mean velocity “for subcritical crack growth between  $c_1$  and  $c_2$  branches” with applied load [56] corresponds to the increase in mean velocity as B' approaches B'.

In the proposed model, acoustic emission occurs only when crack velocity jumps from one positive branch to the other, in agreement with Rose's proposal [73] that acoustic emission corresponds to a crack starting or stopping abruptly. The results of Swindlehurst and Wilshaw [74] show that a single Hertzian cone produces a single emission burst, most probably when the maximum of  $G$  (see Fig. 9) reaches  $G_c$ . Presumably for cones formed at subcritical velocity no acoustic emission would be detected. This is in

apparent contradiction with the results of Evans and Linzer [75], Evans *et al.* [76] and Nadeau [77], showing that the rate of acoustic emission exhibits the same functional dependence on  $K_I$  as does the subcritical velocity, but as shown by Nadeau [77] this acoustic emission is caused by interaction between the moving crack and defects on the surface. No such interaction is expected for a Hertzian cone. Our preliminary results on acoustic emission are in agreement with these ideas.

## 12. Conclusions

The main results obtained in this study are the following:

1. The strain energy release rate for cone fracture under flat axisymmetric punches has been computed and compared with the case of the sphere.
2. The initiation of the crack outside the circle of contact for flat or spherical punches is shown to be due to the steepest gradient of stresses near the circle of contact.
3. The Auerbach range corresponds to the relatively flat maximum of the  $\Phi(c/a)$  curves drawn for various starting radii. In this range only shallow rings are formed ( $c/a < 10^{-1}$ ).
4. The use of Equation 2b gives the same results as Equation 2a for  $c/a < 10^{-1}$ , but considerably improves the results for well-formed cones ( $c/a > 1$ ).
5. A model for subcritical crack growth first proposed for adherence of viscoelastic solids is used. It is assumed that the static fatigue limit corresponds to the true Griffith criterion with intrinsic surface energy  $\gamma$ , whereas  $K_{Ic}$  and  $G_c$  correspond to a point where the crack velocity jumps to higher values because intermediate velocities are unstable. No stress corrosion is needed to explain subcritical crack growth for  $2\gamma < G < G_c$ . The whole  $G(v)$  curve is assumed to be shifted by a change intrinsic surface energy. The experimental results of Mikosza and Lawn [55] are easily interpreted by this model.
6. Experiments on borosilicate glass agree satisfactorily with theory. As the loading system is stopped as soon as subcritical crack growth becomes apparent, application of the Griffith equation gives values of surface energy of about  $4.3 \text{ J m}^{-2}$ , larger than the intrinsic surface energy, and slightly lower than the fracture sur-

face energy derived from higher crack speed experiments.

7. Intrinsic surface energy is better approached by study of well-formed cones, for the crack velocity continuously decreases at constant load. After the load has been on for one hour, application of the Griffith criterion with the Roesler approximation gives an apparent surface energy of  $1.25 \text{ J m}^{-2}$ , whereas preliminary results for the finite element method give  $0.3 \text{ J m}^{-2}$ .

## Appendix

Let us consider an isolated frustum of cone of base  $s$ , height  $z$  and cone angle  $\theta$  (Fig. 5). Under a load  $P$  the elastic displacement obtained by integration of the Hooke law is

$$\delta = \frac{Pz}{\pi Ea(a + z \tan \theta)} \quad (\text{A1})$$

The total energy of the system  $U_E + U_p = \frac{1}{2}P\delta - P\delta$  is thus

$$U = -\frac{P^2 z}{2\pi Ea(a + z \tan \theta)} \quad (\text{A2})$$

The variation of this energy when the lateral surface of the cone extends by  $dA$  can be considered as an approximate value of the strain energy release rate for the cone crack

$$G = -\left(\frac{\partial U}{\partial A}\right)_p \quad (\text{A3})$$

With

$$dA = \frac{2\pi(a + z \tan \theta)}{\cos \theta} dz = \frac{\pi s}{2 \sin \theta} ds \quad (\text{A4})$$

this becomes

$$G = \frac{2 \cos \theta}{\pi^2} \frac{P^2}{Es^3} \quad (\text{A5})$$

The equilibrium given by  $G = 2\gamma$  is stable, since  $G$  decreases as  $s$  increases. For  $\theta = 68^\circ$  this rough approximation gives  $G = 7.6 \times 10^{-2} P^2 / Es^3$ , a value 3.5 times higher than the one given by Roesler [7]. In fact the stresses in the solid below the cone, clearly visible in Culf's photographs [8], have been neglected. Their associated elastic energy increases as  $s$  increases, and should reduce  $g$  if taken into account.

## Acknowledgements

The authors are indebted to the DRET and the GRECO 46 for the financial support of this work. Thanks are due to the referee who proposed Equation 2b for formed cones.

## References

1. F. AUERBACH, *Ann. Phys. Chem.* **43** (1891) 61.
2. M. T. HUBER, *Ann. Physik* **14** (1904) 153.
3. A. E. H. LOVE, *Phil. Trans.* **228** (1929) 377.
4. F. C. FRANK and B. R. LAWN, *Proc. Roy. Soc.* **A299** (1967) 291.
5. B. R. LAWN and T. R. WILSHAW, *J. Mater. Sci.* **10** (1975) 1049.
6. R. WARREN, *Acta Metall.* **26** (1978) 1759.
7. F. C. ROESLER, *Proc. Phys. Soc B* **69** (1956) 981.
8. C. J. CULF, *J. Soc. Glass. Techn.* **41** (1957) 157.
9. J. J. BENBOW, *Proc. Phys. Soc B* **75** (1960) 697.
10. M. V. SWAIN and B. R. LAWN, *Int. J. Fract.* **9** (1973) 481.
11. B. R. LAWN and E. R. FULLER, *J. Mater. Sci.* **10** (1975) 2016.
12. J. S. NADEAU and A. S. RAO, *J. Can. Ceram. Soc.* **41** (1972) 63.
13. I. N. SNEDDON, *Proc. Camb. Phil. Soc.* **42** (1946) 29.
14. M. BARQUINS and D. MAUGIS, *J. Méch. Théor. Appl.* **1** (1982) 331.
15. B. R. LAWN, *J. Appl. Phys.* **39** (1968) 4828.
16. S. WAY, *J. Appl. Mech.* **7** (1940) 147.
17. B. R. LAWN and M. V. SWAIN, *J. Mater. Sci.* **10** (1975) 113.
18. G. I. BARENBLATT, *Adv. Appl. Mech.* **7** (1962) 55.
19. J. R. RICE, "Fracture", Vol. 2, edited by H. Liebowitz (Academic, New York, 1968) p. 222.
20. M. K. KASSIR and G. C. SIH, *J. Appl. Mech.* **33** (1966) 601.
21. F. B. LANGITAN and B. R. LAWN, *J. Appl. Phys.* **40** (1969) 4009.
22. T. R. WILSHAW, *J. Phys. D: Appl. Phys.* **4** (1971) 1567.
23. J. P. A. TILLET, *Proc. Phys. Soc B* **69** (1956) 47.
24. A. S. ARGON, Y. HORI and E. OROWAN, *J. Amer. Ceram. Soc.* **43** (1960) 86.
25. E. W. SUCOV, *ibid.* **45** (1962) 214.
26. B. HAMILTON and H. RAWSON, *J. Mech. Phys. Solids* **18** (1970) 127.
27. K. L. JOHNSON, J. J. O'CONNOR and A. C. WOODWARD, *Proc. Roy. Soc* **A334** (1973) 95.
28. H. CONRAD, M. K. KESHAVAN and G. A. SARGENT, *J. Mater. Sci.* **14** (1979) 1473.
29. H. L. OH and I. FINNIE, *J. Mech. Phys. Solids* **15** (1967) 401.
30. J. S. NADEAU, *J. Amer. Ceram. Soc.* **56** (1973) 467.
31. B. R. LAWN, T. R. WILSHAW and N. E. W. HARTLEY, *Int. J. Fract.* **10** (1974) 1.
32. B. D. POWELL and D. TABOR, *J. Phys. D: Appl. Phys.* **3** (1970) 783.
33. Y. M. TSAI and H. KOLSKY, *J. Mech. Phys. Solids* **15** (1967) 29.
34. F. C. ROESLER, *Proc. Roy. Soc.* **B69** (1956) 55.
35. G. M. C. FISHER, *J. Appl. Phys.* **38** (1967) 1781.
36. J. HARRISON and J. WILKS, *J. Phys. D: Appl. Phys.* **11** (1978) 73.
37. M. K. KESHAVAN, G. S. SARGENT and H. CONRAD, *J. Mater. Sci.* **15** (1980) 839.
38. J. V. LEWIS and H. RAWSON, *Glass Technol.* **17** (1976) 128.
39. H. MATZKE, T. INOUE and R. WARREN, *J. Nucl. Mater.* **91** (1980) 205.
40. H. MATZKE and R. WARREN, *J. Mater. Sci. Lett.* **1** (1982) 441.
41. U. C. B. O. EJIKE, *J. Elast.* **11** (1981) 359.
42. D. MAUGIS and M. BARQUINS, *J. Phys. D: Appl. Phys.* **16** (1983) 1843.
43. R. E. MOULD, *J. Amer. Ceram. Soc.* **43** (1960) 160.
44. R. E. MOULD and R. D. SOUTHWICK, *ibid.* **42** (1959) 582.
45. E. K. PAVELCHEK and R. H. DOREMUS, *J. Mater. Sci.* **9** (1974) 1803.
46. D. N. TURNER, P. D. SMITH and W. B. ROTSEY, *J. Amer. Ceram. Soc.* **50** (1967) 594.
47. M. M. CHAUDHRI and E. H. YOFFE, *Phil. Mag.* **A44** (1981) 667.
48. H. MATZKE, *J. Mater. Sci.* **15** (1980) 739.
49. J. A. GREENWOOD and J. H. TRIPP, *J. Appl. Mech.* **89** (1967) 153.
50. F. C. YIP and J. E. S. VENART, *J. Phys. D: Appl. Phys.* **4** (1971) 1470.
51. K. L. JOHNSON, "The mechanics of the contact between deformable bodies", edited by A. D. De Pater and J. J. Kalker (Delft University Press, Rotterdam, 1975) p. 26.
52. B. D. HUGHES and L. R. WHITE, *Trans. ASME* **47** (1980) 194.
53. J. KAGAMI, K. YAMADA and T. HATAZAWA, *Wear* **87** (1983) 93.
54. F. B. LANGITAN and B. R. LAWN, *J. Appl. Phys.* **41** (1970) 3357.
55. A. G. MIKOSZA and B. R. LAWN, *ibid.* **42** (1971) 5540.
56. B. R. LAWN, "The science of hardness testing and its research applications", edited by J. H. Westbrook and H. Conrad (ASM, Metals Park, 1973) p. 418.
57. D. MAUGIS, *J. Mater. Sci.* **20** (1985) in press.
58. D. MAUGIS and M. BARQUINS, *J. Phys. D: Appl. Phys.* **11** (1978) 1989.
59. *Idem*, "Adhesion and adsorption of polymers", Part A, edited by L. H. Lee (Plenum, New York, 1980) p. 203.
60. A. N. GENT and J. SCHULTZ, *J. Adhes.* **3** (1972) 281.
61. E. H. ANDREWS and J. A. KINLOCH, *Proc. Roy. Soc.* **A332** (1973) 385.
62. D. MAUGIS, "Microscopic aspects of adhesion and lubrication", edited by J. M. Georges (Elsevier, Amsterdam, 1982) p. 221.
63. S. M. WIEDERHORN, E. R. FULLER and R. THOMSON, *Met. Sci.* **14** (1980) 450.
64. S. M. WIEDERHORN, *J. Amer. Ceram. Soc.* **52** (1969) 99.

65. S. M. WIEDERHORN, H. JOHNSON, A. M. DINESS and A. H. HEUER, *ibid.* **57** (1974) 336.
66. S. M. WIEDERHORN and L. H. BOLTZ, *ibid.* **53** (1970) 543.
67. S. M. WIEDERHORN, "Fracture Mechanics of Ceramics", Vol 2, edited by R. C. Bradt, D. P. H. Hasselman and F. F. Lange (Plenum, New York, 1974) p. 613.
68. A. J. HOLLAND and W. E. S. TURNER, *Glass Technol.* **24** (1940) 46T.
69. M. V. SWAIN, J. S. WILLIAMS, B. R. LAWN and J. J. H. BEEK, *J. Mater. Sci.* **8** (1973) 1153.
70. A. G. METCALFE and G. K. SCHMITZ, *Glass Technol.* **13** (1972) 5.
71. T. P. DABBS and B. R. LAWN, *J. Amer. Ceram. Soc.* **65** (1982) C37.
72. S. M. WIEDERHORN, A. G. EVANS and D. E. ROBERTS, "Fracture Mechanics of Ceramics", Vol. 2, edited by R. C. Bradt, D. P. H. Hasselman and F. F. Lange (Plenum, 1974) p. 829.
73. L. R. F. ROSE, *Int. J. Fract.* **17** (1981) 45.
74. W. E. SWINDLEHURST and T. R. WILSHAW, *J. Mater. Sci.* **11** (1976) 1653.
75. A. G. EVANS and M. LINZER, *J. Amer. Ceram. Soc.* **56** (1973) 575.
76. A. G. EVANS, M. LINZER and L. R. RUSSEL, *Mater. Sci. Engng* **15** (1974) 253.
77. J. S. NADEAU, *J. Amer. Ceram. Soc.* **64** (1981) 585.

*Received 25 May  
and accepted 18 December 1984*